Dispersive Wave Focusing on a Shear Current: Part 1-Linear Approximations

Simen Å. Ellingsen, Zibo Zheng, Malek Abid, Christian Kharif, Yan Li

Dispersive wave focusing on a shear current. Part 1: Linear approximations

Simen Å. Ellingsen[1*†], Zibo Zheng[1†], Malek Abid[2], Christian Kharif[2] and Yan Li[3]

[1]Department of Energy and Process Engineering, Norwegian University of Science and Technology, Trondheim,7491,Norway.
[2] Institut de Recherche sur les Phénomènes Hors Equilibre, Aix-Marseille Université, Marseille, 13384, France.
[3]Department of Mathematics, University of Bergen, Bergen, 5007, Norway.

*Corresponding author(s). E-mail(s): simen.a.ellingsen@ntnu.no;
†SÅE and ZZ are to be considered joint first authors.

Abstract

We consider the evolution and kinematics during dispersive focusing, for a group of waves propagating atop currents varying with depth. Our analysis assumes long-crested linear waves propagating at arbitrary angles relative to the current. Although low steepness is assumed, the linear model is often a reasonable approximation for understanding rogue waves. A number of analytical approximate relations are derived assuming different sub-surface current profiles, including linearly varying current, exponentially varying current, and currents of arbitrary depth profile which are weakly sheared following the approximation of Stewart & Joy (*Deep Sea Res. Abs.* **21**, 1974). The orbital velocities are likewise studied. While shear currents have modest influence on the motion of the envelope of the wave group, they significantly change wave kinematics. Horizontal orbital velocities are either amplified or suppressed depending on whether the shear is opposing or following, respectively. To illustrate these phenomena we consider a real-world example using velocity profiles and wave spectra measured in the Columbia River estuary. Near the surface at the point where focusing occurs, horizontal orbital velocities are respectively increased and decreased by factors of **1.4** and **0.7** for focusing groups propagating on following and

opposing shear (respectively upstream and downstream in the earth-fixed reference system). The implications for the forces a focusing wave group can exert on vessels and installations are profound, emphasizing the importance of considering current profiles in maritime operations.

Keywords: Wave-shear current interaction, Focused wave group, Wave kinematics

1 Introduction

Rogue waves, characterized as enormous and abrupt waves appearing on the sea's surface, pose a significant threat to maritime activities. These waves which are defined by being far higher than the waves around them, can emerge without warning, occurring both in deep and shallow waters, and they result from various physical mechanisms that concentrate the energy of water waves into a small area. Their occurrence has led to numerous fatalities, injuries, and extensive damages to ships and maritime structures. Among the mechanisms responsible for their formation are dispersive focusing, refraction influenced by variable currents and bottom topography, modulational instability, constructive wave interference enhanced by second-order interactions, cross-sea interactions, and soliton interactions. For a comprehensive review of these mechanisms, refer to the works by Kharif & Pelinovsky [1], Dysthe et al. [2], and Onorato et al. [3].

The main objective of this paper is to analyze the effect of depth-dependent underlying currents on the dispersive focusing of water waves in deep water. Extreme wave events resulting from dispersive focusing or spatiotemporal focusing phenomena can be described as follows: when initially shorter wave packets are positioned in front of longer wave packets with higher group velocities, the longer waves eventually catch up and overtake the shorter waves during the dispersive evolution process. At a fixed location (known as the focus point) and time, the superposition of all these waves leads to the formation of a large-amplitude wave. Subsequently, the longer waves move ahead of the shorter waves, resulting in a decrease in the amplitude of the wave train. In the absence of vorticity, giant waves created by dispersive focusing have been frequently studied experimentally [4–7] and theoretically [8, 9], but studies in the presence of a shear current are very scarce. Kharif et al. [10] investigated the effect of a constant vorticity underlying current on the dispersive focusing of a one-dimensional nonlinear wave group propagating in shallow water. Their findings revealed that the presence of constant vorticity increases the maximum amplification factor of the surface elevation as the shear intensity of the current increases. The duration of extreme wave events follows a similar behavior. In narrowband assumption Xin et al. [11] report the different effects of following and opposing shear current on both the extreme and fatigue loads on fixed-bottom offshore slender structures in extreme wave events. The work

has shed light on the shear-current modified wave kinematics in the design of offshore structures, which will be explored further in this work as explained below.

This study is the first part of an investigation of waves focusing dispersively on vertically sheared currents. The, in some respects, simplest case is treated in this first part, where the theory is linearised with respect to wave steepness; a second-order theory is found in part two [12]. Although nonlinear wave effects are significant for rogue wave situations, a linear approximation has been found to give reasonable results [13]. Our focus is on investigating the behavior of focusing wave groups propagating obliquely to the current direction, as well as wave groups traveling in the same direction as the current, in deep water (see Figure 1). By analyzing the impact of these depth-dependent underlying currents on the dispersive focusing of water waves, we aim to enhance our understanding of the formation and characteristics of rogue waves, contributing to improved safety measures for maritime activities as highlighted in [11].

We consider a range of vertically sheared currents, and of wave shapes at focus, deriving a series of closed-form approximate results. The currents we consider include the linear and exponential depth dependence — cases for which closed-form solutions exist for the linear velocity field — and arbitrary current profiles which satisfy the weak-shear approximation (fundamentally that required for the celebrated approximation of Stewart & Joy [14]). Wave groups focusing to a δ-function singularity, and a narrowband Gaussian packet, are considered. The approximate formulae derived are, we propose, useful for their relative simplicity and analytical tractability, for instance for the creation of focusing waves on sheared currents in numerical and laboratory experiments (see, e.g., [15]).

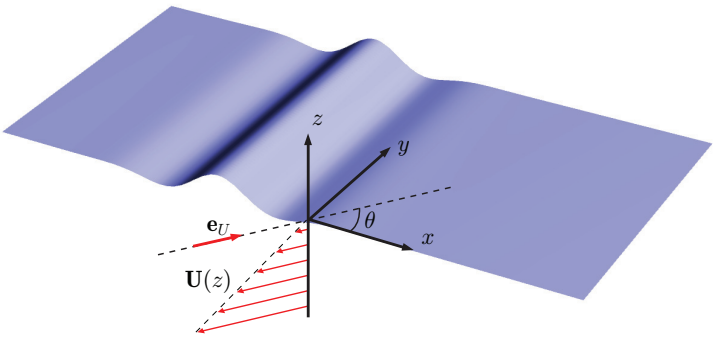

Fig. 1 Geometry: a quasi-2D wave propagating along the x axis. A sub-surface shear current makes an angle θ with the direction of wave propagation. Here $\mathbf{U}(z) = Sz\mathbf{e}_U$. Currents with opposing and following shear are denoted by $\theta \in [0, \pi/2)$ and $(\pi/2, \pi]$, respectively.

A main conclusion of our work, illustrated and quantified through many examples, is the following: within a linear framework, the presence of shear has modest effect on the focusing and defocusing of the wave-group envelope, but

a large effect on the wave kinematics. The component of the orbital velocities near the surface at the point of focus can be strongly enhanced.

2 Theoretical background

In this section we review the necessary background theory and phrase it in the formalism we use herein. While not in a strict sense novel, the reexamination of the basics sheds important light on the mechanisms in play which we will refer extensively to in later sections. After defining the problem and geometry, the linear initial-value solution is provided in a suitable form, and standard current profiles and highly useful approximations are briefly recapitulated.

2.1 Problem definition

We consider a body of water with a free surface which, when undisturbed, is at $z = 0$, and sustaining a shear current which depends arbitrarily on depth. The depth is infinite (some results are generalised to allow finite depth in Appendix A), and we ignore the effects of surface tension. The geometry is sketched in figure 1. The background current has the form

$$\mathbf{U}(z) = \{U_x(z), U_y(z)\} = U(z)\mathbf{e}_U; \tag{1}$$

$$\mathbf{e}_U = \{\cos\theta, \sin\theta\}, \tag{2}$$

where $\mathbf{e}_U$ is a unit vector in the xy plane. Without loss of generality we choose the coordinate system which follows the surface of the water so that $U(0) = 0$. As well as simplifying the formalism this choice emphasizes that the effects studies are due to shear rather than surface current. A nonzero surface current is easily worked back into solutions by adding a Doppler shift to frequencies. The angle between wave propagation and current is θ and we shall assume without loss of generality that the wave propagates along the x axis so that $\mathbf{k} \cdot \mathbf{U} = kU_x = kU(z)\cos\theta$. In derivations we shall often retain a general wave vector $\mathbf{k} = \{k_x, 0\}$. We allow k_x to take both signs in derivations, eventually arriving at expressions for waves propagating only in the positive x direction, whereupon we may consider only positive wave numbers. We assume long-crested waves, so the surface elevation is $\zeta(\mathbf{r}, t) = \zeta(x, t)$ where $\mathbf{r} = (x, y)$. We assume here that the current does not change direction with depth, but generalisation to a z-dependent θ is straightforward.

As is well known (e.g. [16]), the surface elevation and dispersion relation depend only on $\mathbf{U}$ in the combination $\mathbf{k}\cdot\mathbf{U} = kU_x$, whereas U_y has no influence on ζ. The angle θ thus only plays the role of varying U_x through values between $-U$ and U. We shall see in section 4 that the same is not the case for the velocity field beneath the waves.

In this paper we linearise equations and boundary conditions with respect to ζ and its derivatives, as well as orbital velocities — a companion paper considers weakly nonlinear extensions.

2.2 Linear initial-value problem, and solution

We will solve initial value problems in this set-up, a simpler, long-crested version of the theory presented in [17]. The general linear solution can be written in Fourier form with the 3D formulae in Ref. [17] assuming translational symmetry in the y direction, as

$$\zeta(\mathbf{r},t) = \int_{-\infty}^{\infty} \frac{\mathrm{d}k_x}{2\pi}\Big[b_+(k_x)e^{-i\omega_+(k_x)t} + b_-(k_x)e^{-i\omega_-(k_x)t}\Big]e^{ik_x x} \tag{3}$$

where $\omega_\pm(\mathbf{k})$ are the two solutions of the linear dispersion relation for a general wave vector $\mathbf{k}$, and $b_\pm(\mathbf{k}) = b_\pm(k_x)$ are spectral weights determined by initial conditions.

In the reference system following the surface current (i.e., $U(0) = 0$), the dispersion relation always has one positive and one negative solution, corresponding to waves propagating in direction $\mathbf{k}$ and $-\mathbf{k}$, respectively, implying that $\omega_+ \geq 0$ and $\omega_- \leq 0$.

Our initial condition is that the shape of the packet is prescribed at focus, $t = 0$, and propagates only in the positive x direction. Let the Fourier transform of ζ at focus be

$$\zeta(x,0) = \int_{-\infty}^{\infty} \frac{\mathrm{d}k_x}{2\pi}\tilde{\zeta}_0(k_x)e^{ik_x x}; \quad \tilde{\zeta}_0(k_x) = \int_{-\infty}^{\infty} \mathrm{d}x\, \zeta(x,0)e^{-ik_x x}, \tag{4}$$

which with the general linear solution (3) implies

$$b_+(k_x) + b_-(k_x) = \tilde{\zeta}_0(k_x). \tag{5}$$

In order to obtain the appropriate initial shape with only plane waves propagating in the $+x$ direction, we couple the kernel $\exp(ik_x x)$ to $\exp(-i\omega_- t)$ when $k_x < 0$ and to $\exp(-i\omega_+ t)$ when $k_x > 0$:

$$b_\pm(k_x) = \tilde{\zeta}_0(k_x)\Theta(\pm k_x), \tag{6}$$

where Θ is the Heaviside unit step function, explicitly

$$\tilde{\zeta}_0(k_x,t) = \tilde{\zeta}_0(k_x)\left[e^{-i\omega_-(k_x)t}\Theta(-k_x) + e^{-i\omega_+(k_x)t}\Theta(k_x)\right]. \tag{7}$$

Substituting $k_x \to -k_x$ for the b_- term and noticing the well-known symmetry

$$\omega_-(-k_x) = -\omega_+(k_x), \tag{8}$$

the solution may be written

$$\zeta(x,t) = \int_0^{\infty} \frac{\mathrm{d}k}{2\pi}\Big[\tilde{\zeta}_0(-k)e^{-i\psi} + \tilde{\zeta}_0(k)e^{i\psi}\Big], \tag{9}$$

where we now simplify the notation, $k_x \to k$ and $\omega_+(k_x) \to \omega(k)$ is the positive-valued frequency. As shorthand, we define the wave phase

$$\psi = \psi(x,t;\ k) \equiv kx - \omega(k)t, \tag{10}$$

frequently written without arguments for succinctness. Since (9) is real-valued, it follows that $\tilde{\zeta}_0(-k) = \tilde{\zeta}_0^*(k)$, so we finally write

$$\zeta(x,t) = 2\,\mathrm{Re}\int_0^\infty \frac{\mathrm{d}k}{2\pi}\tilde{\zeta}_0(k)e^{i\psi}. \tag{11}$$

In the following we shall use this form and therefore assume $k_x = k > 0$, with the exception of derivations where it is sometimes necessary to return to the more fundamental form.

In particular, if the shape at $t = 0$ is symmetrical around $x = 0$, $\tilde{\zeta}_0(k)$ is real, hence

$$\zeta(x,t) = 2\int_0^\infty \frac{\mathrm{d}k}{2\pi}\tilde{\zeta}_0(k)\cos\psi(x,t;\ k). \tag{12}$$

2.3 Vertically sheared currents

We here introduce the classic linear and exponential shear profiles used as canonical examples, and approximate linear theories for arbitrary shear. Known results are briefly reviewed and framed in the formalism we use herein.

2.3.1 Current with constant shear

First we quote well-known results for the simple, linearly depth-dependent current

$$\mathbf{U}(z) = Sz\mathbf{e}_U = Sz\{\cos\theta, \sin\theta\} \tag{13}$$

with S the constant shear.

Due to the symmetry (8) it is sufficient to consider the positive-valued $\omega(k)$ assuming positive k, which we write in the form

$$\omega_\sigma(k) = kc_\sigma(k) = \sqrt{g\varkappa} - \sigma \tag{14}$$

where the shear-modified wave number is

$$\varkappa(k) = k + \sigma^2/g, \tag{15}$$

and

$$\sigma \equiv \tfrac{1}{2}S\cos\theta. \tag{16}$$

The group velocity is

$$c_{g\sigma}(k) = \frac{1}{2}\sqrt{\frac{g}{\varkappa}}. \tag{17}$$

Note for future reference that $c_{g\sigma}(k)$ is symmetrical under $\sigma \to -\sigma$ while c_σ is not.

In the spirit of [17, 18] we may define a Froude-shear number for the linear-shear current based on velocity S/k and length $1/k$,

$$\mathrm{FS}_{\mathrm{lin.}} = \frac{S}{2\sqrt{gk}} \tag{18}$$

so that the shear-modified wave number is $\varkappa = k(1 + \mathrm{FS}^2_{\mathrm{lin.}} \cos^2\theta)$. This is particularly instructive in narrow-band cases (e.g., long groups with Gaussian envelope) where there is a dominating carrier wave number; see sections 3.4 and 4.1 for further details. Here and henceforth a subscript 'lin.' indicates the subscribed quantity pertains to the linear current.

2.3.2 Current with exponential shear

We will frequently make use of the model current with exponential depth profile, which we define

$$\mathbf{U}_{\exp}(z) = U_0(\mathrm{e}^{\alpha z} - 1)\mathbf{e}_U = \{U_{x0}, U_{y0}\}(\mathrm{e}^{\alpha z} - 1), \tag{19}$$

where $\alpha > 0$ is a shear strength and U_{x0} a current strength. This model has been considered for the purposes of wave-current interactions for a very long time, thanks to its similarity to a wind-driven shear-layer (Ekman current) [19].

An explicit, exact solution to the linear problem with the exponential current can be found in terms of hypergeometric functions, which we review in section 4.4. The dispersion relation in this case is, however, implicit but easily calculated numerically.

The exponential profile is a particularly useful model in combination with the weak-shear approximation (see section 2.4.1), an approximation which is excellent in the vast majority of oceanographic and coastal flows. Near-surface flows, such as wind-driven Ekman layers or estuarine plumes, are typically reasonably approximated by an exponential, and in this case the linearised weak-shear theory yields a wealth of explicit analytical results, a number of which we derive in this article.

2.4 Weak-shear and weak-curvature theory

We will summarise the results of theories for dispersion relations and flow fields for an arbitrary current $\mathbf{U}(z)$ satisfying criteria of weak shear and weak curvature, respectively. We emphasize that although the former approximation is termed 'weak shear' due to the formal requirements for it to be asymptotically accurate, in fact in an oceanic setting the shear can be very strong as in the case of the Columbia River Estuary considered in section 4.5.1, and still give results accurate to within a few percent or less.

The weak-shear approximation is in practice that underlying the celebrated approximation of Stewart & Joy [14], typically sufficient in practice while in

cases of extremely strong shear (as effectively felt by a wave of the wavelength in question), the strong-shear-weak-curvature expressions [20] could be necessary.

As discussed in Ref. [20], a suitable measure of the effective strength of the current shear is a dimensionless depth-integrated shear, or "directional shear-Froude number", $\delta(\mathbf{k})$, defined as

$$\delta(\mathbf{k}) \equiv \frac{1}{c_0(k)} \int_{-\infty}^{0} \mathrm{d}z\, U_x'(z) \mathrm{e}^{2kz} \equiv \mathrm{FS}_{\mathrm{gen.}} \cos\theta. \tag{20}$$

with $c_0(k) = \sqrt{g/k}$ as usual. We use the symbol δ as well as FS to make contact with previously published theory [17, 18, 20], despite the slight redundancy. The x component of $\mathbf{U}$ is taken, being the component aligned with the waves, $\mathbf{k} \cdot \mathbf{U} = kU_x$.

That the parameter $\delta(\mathbf{k})$ is a direct generalisation of the shear-Froude number (18) for linear shear based on the along-wave (here: x) current component, is easily seen by inserting $U_x(z) = Sz\cos\theta = 2\sigma z$ which gives $\delta(\mathbf{k}) = \delta_{\mathrm{lin.}}(\mathbf{k})$ with

$$\delta_{\mathrm{lin.}}(\mathbf{k}) = 2\sigma\sqrt{\frac{k}{g}} \int_{-\infty}^{0} \mathrm{d}z\, \mathrm{e}^{2kz} = \frac{\sigma}{\sqrt{gk}} = \mathrm{FS}_{\mathrm{lin.}} \cos\theta. \tag{21}$$

For ease of comparison to the linear-shear case above, it is also instructive for us to define the shear-induced Doppler shift for a wave propagating at an angle θ:

$$\sigma_\delta(k) = \omega_0(k)\delta(\mathbf{k}) = k \int_{-\infty}^{0} \mathrm{d}z\, U_x'(z) \mathrm{e}^{2kz} \tag{22}$$

a generalisation of σ for the linear current in Eq. (16). We defined $\omega_0 = \sqrt{gk}$.

2.4.1 Weak shear

A sufficient criterion for the approximate theory of Stewart & Joy [14] and its generalisations [21, 22] to be accurate is $\delta(\mathbf{k}) \ll 1$ for all k which contribute significantly (we follow the convention of [23] that $\ll$ and $\gg$ refer to the absolute values of the quantities compared). The results in references [14, 22] were derived assuming weak current, $U \ll c$, yet it is shown in ref. [20] that the true condition of validity is that the shear is weak. (This was suspected by Kirby & Chen [22] and in fact obliquely discussed already by Skop [21]). After a partial integration of the original form of the much-used approximation due to Stewart & Joy [14], it can be written

$$\omega(k) \approx \sqrt{gk} - \sigma_\delta(k) = \omega_0(k)[1 - \delta(\mathbf{k})]. \tag{23}$$

We mention in passing that although (20) performs excellently for most typical ocean and coastal currents concentrated in the near-surface region (e.g. [20,

24]), such as the exponential current profile, it does not perform particularly well for the linear shear case even when shear is moderate [24]; for currents which are close to linear, the strong-shear approximation in the next section should be used.

Further formulae in the weak-shear approximation will be quoted or derived later, as they are needed. Explicit expressions for the exponential current in the context of surface motion are found in section 3.2.1, and weak-shear theory for the kinematics and orbital velocities may be found in Section 4.2.

2.4.2 Strong shear, weak curvature

A similar theory allowing $U(z)$ to have arbitrarily strong shear, but weak curvature, was developed by Ellingsen & Li [20]; the explicit limitation on curvature may be found therein. Now $\delta(\mathbf{k})$ can be arbitrarily large compared to unity. The approximate dispersion relation derived in [20] (equation 18) is

$$\omega(k) \approx \omega_0(k)(\sqrt{1+\delta^2} - \delta) = \sqrt{gk + \sigma_\delta^2} - \sigma_\delta. \tag{24}$$

Ellingsen & Li finds no practical situations where (24) performs significantly worse than (23), and it fares far better when δ is not small compared to unity. Notice that when the linear current (13) is inserted, one finds $\sigma_\delta(k) = \sigma$ as defined in (16) and the dispersion relation (14) is regained exactly. The formalism thus bears a close similarity to that with constant shear, in section 2.3.1. Moreover, $\delta \ll 1$ returns the weak-shear dispersion relation (23) to leading order.

The close resemblance in form to the constant shear case makes it natural to define a generalised function analogous to Eq. (15),

$$\varkappa_\delta(k) = k + \sigma_\delta(k)^2/g. \tag{25}$$

whereby (24) can be written $\omega(k) \approx \omega_\delta(k) = \sqrt{g\varkappa_\delta(k)} - \sigma_\delta(k)$.

3 Surface motion

In this section we derive and analyse a number of potentially useful results for the moving free surface of a focusing wave groups, including explicit approximate expressions for general and special cases. We assume throughout in Section 3 that the surface elevation at focus, $\zeta(x, 0)$, is symmetric in x for simplicity.

For purposes of analytical treatment, there are two challenges to contend with when a vertical shear current is present: the dispersion relation is not in general given in closed form, and the waves are described by Fourier integrals with no closed-form solutions. We consider in the following a number of special cases and/or simplifying assumptions which allow useful, closed-form expressions to be derived.

3.1 General dispersion considerations

We briefly argue why the dispersion relation predicts that vertical shear of $U(z)$ has little effect on the group envelope, but can greatly affect the phase velocity and hence the wave kinematics. We focus now on the simplest case of a linear shear current (13) which is sufficient to illustrate the overall effect of shear.

If now σ is not small compared to $\sqrt{k}$, the phase velocity in equation (14) depends strongly on θ; for $\cos\theta > 0$ (opposing shear) the two terms in (14) tend to cancel each other while for $\cos\theta < 0$ (following shear) they add to each other, giving a phase velocity which can be far higher. In contrast, the group velocity is identical under $\theta \to -\theta$ since $c_{g\sigma}$ depends on $|\cos\theta|$ only.

Bearing in mind that the envelope of a focusing group of waves is governed by the group velocity and its k derivative, the evolution of the group as a whole is largely independent of whether propagation is upstream or downstream. The kinematics of the wave patterns within the focusing group, however, are related to the phase velocity which can be very different depending on the direction θ. To wit, the ratio between phase velocity for opposite directions $\theta = 0$ and $\theta = \pi$ is

$$\frac{c(\theta=\pi)}{c(\theta=0)} = \frac{\sqrt{1+\mathrm{FS}_{\mathrm{lin.}}^2}+\mathrm{FS}_{\mathrm{lin.}}}{\sqrt{1+\mathrm{FS}_{\mathrm{lin.}}^2}-\mathrm{FS}_{\mathrm{lin.}}} = \left(\sqrt{1+\mathrm{FS}_{\mathrm{lin.}}^2}+\mathrm{FS}_{\mathrm{lin.}}\right)^2 \tag{26}$$

which very significant indeed when $\mathrm{FS}_{\mathrm{lin.}} \sim \mathcal{O}(1)$. In section 4 we study the closely related amplification of horizontal velocities at focus depending on θ.

The situation becomes particularly pointed for strong shear, $\sigma \gg 1$, in which case the phase and group velocities in equations (14) and (17) are

$$c_\sigma(k) = \frac{1}{k}(|\sigma|-\sigma) + \frac{g}{2|\sigma|} + \ldots \tag{27a}$$

$$c_{g\sigma}(k) = \frac{g}{2|\sigma|} + \ldots \tag{27b}$$

For $\cos\theta > 0$ the group and phase velocities become asymptotically equal and the wave becomes nondispersive, whereas for $\cos\theta < 0$ phase velocity can be many times greater than group velocity.

The effect is illustrated in Fig. 2 where we plot $\eta(x,t)$ at a series of equidistant times as the wave group focuses and defocuses. A short Gaussian packet with carrier wave number k_0 and length L is chosen for improved illustration, as defined and discussed in section 3.4. We plot time in units of $T_{\mathrm{ref}} = \sqrt{L/g}$. The surface elevation $\zeta(x,t)$ was evaluated numerically from Eq. (12). The shear S is constant and made strong for clarity of illustration, $\mathrm{FS}_{\mathrm{lin.}}\cos\theta$ takes the values $-\frac{1}{2}, 0$ and $\frac{1}{2}$ at $k = k_0$. When $\theta = 0$ focusing is characterised by a wave group which slowly varying phase as the group passes through focus. When $\theta = \pi$ on the other hand, crests and troughs move so rapidly that they

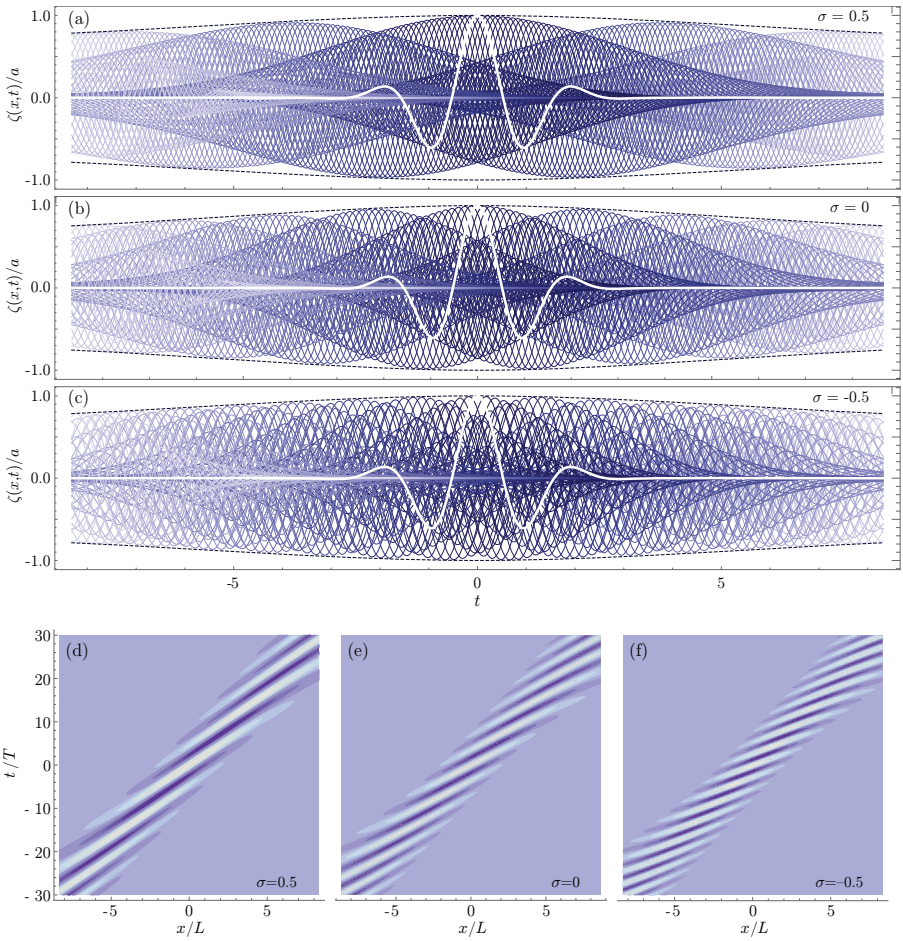

Fig. 2 Illustration of the different kinematic behaviour for waves focusing into a short group, $k_0 L = 3$ with a Gaussian envelope of standard deviation L in deep water for opposing, zero and following linear shear. (a,b,c): $\zeta(x,t)/a$ for $\tilde{t}$ from -30 to 30 in steps of 0.25 with graphs growing progressively lighter in colour for increasing $|t|$, and the $t = 0$ (focused) wave group drawn as thicker white lines. The dashed lines are plots of the maximum group height, $\pm L(L^4 + B_0^2 t_g(x)^2)^{-1/4}$, using Eqs. (56), (54) and $t_g(x) = x/c_g(k_0)$. (d,e,f): same, with ζ as shades from darkest to lightest ($\zeta/a = -1$ and $\zeta/a = 1$, respectively), varying in space and time.

appear almost chaotic at this time resolution. (An illustration of the shallow water case is given in A.3.)

Another case suitable for illustration is the wave which takes the form of a Gaussian soliton at focus,

$$\zeta(x,0) = a e^{-x^2/2L^2}; \quad \tilde{\zeta}_0(k) = \sqrt{2\pi} a L e^{-\frac{1}{2}k^2 L^2}. \tag{28}$$

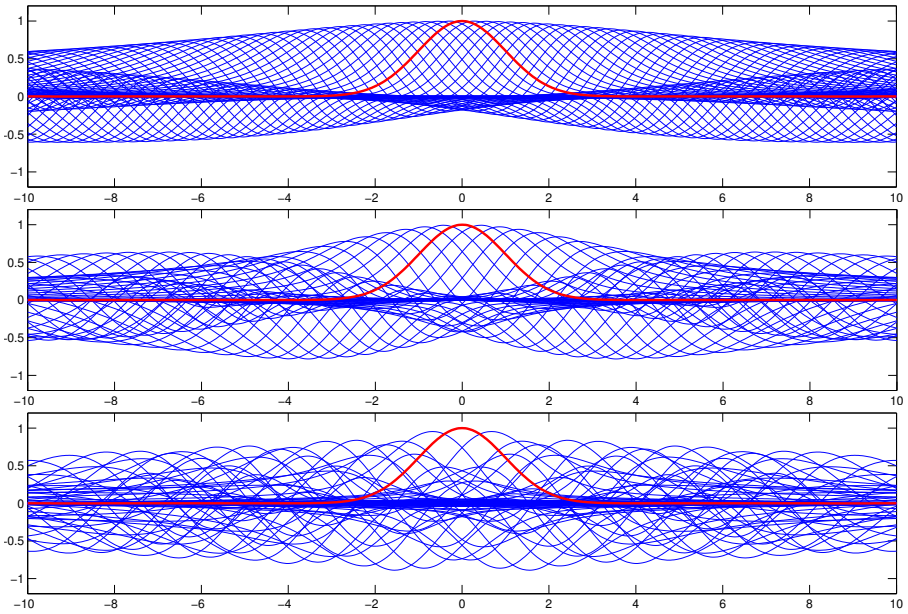

Fig. 3 Illustration of the different kinematic behaviour for waves focusing into a Gaussian soliton of nondimensional width 1 in deep water. The solid graphs show $\zeta(x,t)/a$ for $t/T_{\rm ref}$ from -20 to 20 in steps of 0.5. Here $T_{\rm ref}\sigma = 1, 0$ and -1 (top to bottom). The abcissa is x/L, and $\zeta(x,0)/a$ is shown with thicker, red line.

the width of the Gaussian focused shape. The shape is considered by [25], where an explicit solution is found in the shallow-water case without shear. The surface elevation according to Eq. (12) is

$$\zeta(x,t) = \sqrt{\frac{2}{\pi}} aL\,\mathrm{Re}\left[\int_0^\infty \mathrm{d}k\, e^{-\frac{1}{2}k^2L^2 + ikx - i\omega(k)t}\right]. \tag{29}$$

The time evolution of a group focusing into a Gaussian soliton with constant shear in deep water is shown in Fig. 3. The behaviour is once again that the wave group focusing on following shear ($\cos\theta = -1$) and that on opposing shear ($\cos\theta = 1$), while sharing the same averaged envelope, behave quite differently in a kinematic sense, the former appearing as a single soliton rising slowly to its maximum and declines again, whereas the latter draws a hectic picture of crests and troughs rapidly replacing each other as the focus is approached.

3.2 Stationary phase approximations

Before considering particular cases we derive a general expression for the stationary phase approximation of the shape of the wave packet sufficiently far from focus. Assume therefore that $x, t \gg 1$. Formally we write $\psi = t(k\xi - \omega(k))$

where

$$\xi \equiv x/t, \tag{30}$$

and we assume ξ is moderately large, in the order of $c_g(k)$, then take the asymptotic solution as $|t| \to \infty$ [23].

Equation (12) is rapidly oscillating and dominated by its stationary points when $|t| \to \infty$. We presume for simplicity that only one such exists, which is the case for for gravity waves except very special and extreme cases; should several stationary points exist, the procedure is simply repeated for each one. Equation (12) has its stationary point at $k = k_{\rm sp}$ which solves $\psi'(k_{\rm sp}) = 0$ where a prime here denotes differentiation w.r.t. k. This implies $c_g(k_{\rm sp}) = \xi$ with $c_g(k_{\rm sp})$ being the stationary-point group velocity. In general the stationary point must be found numerically, for example with the Direct Integration Method [26] which we will employ later.

Now let a subscript 'sp' indicate the quantity is evaluated at $k = k_{\rm sp}$. To connect with formalism in following sections (equation (54) in particular), we define

$$A_{\rm sp} = \left.\frac{{\rm d}\omega}{{\rm d}k}\right|_{k=k_{\rm sp}}; \qquad B_{\rm sp}(\xi) = \left.\frac{{\rm d}^2\omega}{{\rm d}k^2}\right|_{k=k_{\rm sp}}. \tag{31}$$

Clearly, $A_{\rm sp} = \omega'_{\rm sp} = c_g(k_{\rm sp}) = \xi$, and $\psi''_{\rm sp} = -\omega''_{\rm sp} t = -B_{\rm sp}(\xi)t$ (note that $B_{\rm sp}$ is a function of ξ because $k_{\rm sp}$ is). With the stationary phase approximation (e.g., §6.5 of [23])

$$\begin{aligned}\zeta(x,t) =& {\rm Re}\left\{\frac{1}{\pi}\int_0^\infty {\rm d}k\, \tilde{\zeta}_0(k){\rm e}^{i\psi(x,t;\,k)}\right\}\\ \approx& \sqrt{\frac{2}{\pi|B_{\rm sp}(\xi)t|}}\,{\rm Re}\left\{\tilde{\zeta}_0(k_{\rm sp})\exp\left[i(\psi_{\rm sp} + \tfrac{\pi}{4}{\rm Sg}(x))\right]\right\}\Theta(\xi \geq c_{g,\min}),\end{aligned} \tag{32}$$

where 'Sg' denotes the sign function, Θ is the unit step function, and $c_{g,\min}$ is the smallest value $c_g(k)$ can take. In particular, solutions only exist for $\xi > 0$ (bear in mind the assumption $\xi/c_g \sim 1$).

In all cases in the following, ${\rm Sg}[\psi''_{\rm sp}] = {\rm Sg}(x) = {\rm Sg}(t)$ when a stationary point exists, which we therefore assume henceforth.

3.2.1 Stationary phase approximation, exponential shear

Consider next the case of an exponential current, equation (19). The weak-shear approximation is sure to be accurate in any direction θ if $\delta(\mathbf{k}) \ll 1$ where, from equation (20), $\delta(\mathbf{k}) = \delta_\alpha(\mathbf{k})$ with w

$$\delta_\alpha(\mathbf{k}) = \frac{U_{x0}}{c_0(k)}\frac{\alpha}{\alpha + 2k}. \tag{33}$$

We might equally refer to δ_α as the Froude-shear number for the exponential case (notation ${\rm FS}_{\rm exp}\cos\theta = \delta_\alpha$, although we will use δ_α in the following).

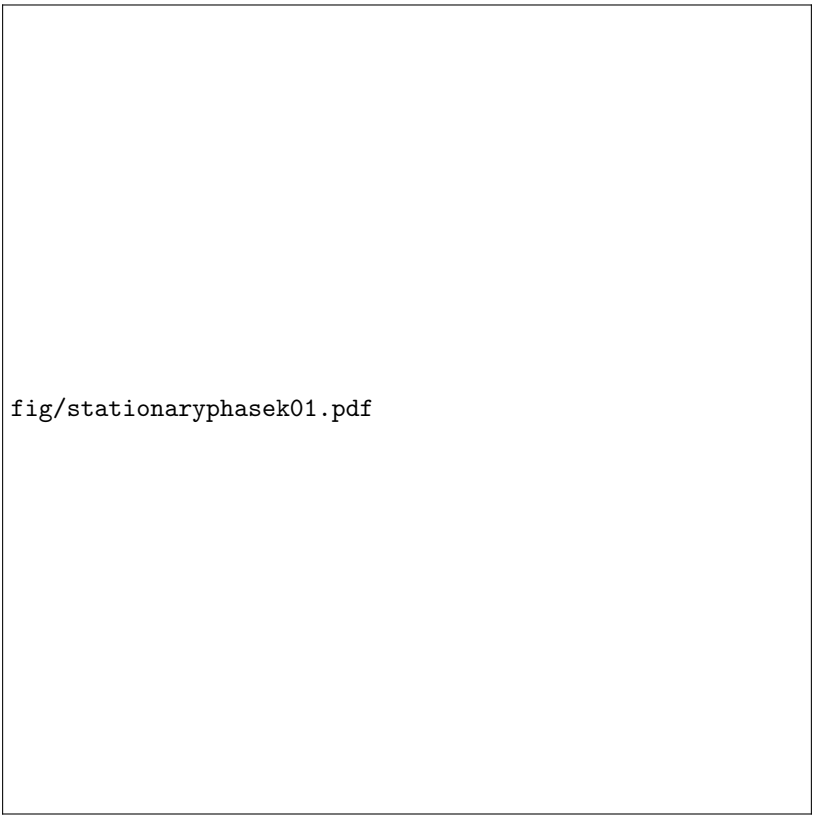

Fig. 4 Wave surface elevation on an exponential shear current (19) with $U_0/\sqrt{gL} = 0.2$, $\alpha L = 2.5$ and $\theta = 0$. The red dashed line is the stationary phase approximation (32) with the weak exponential shear approximation using equations (35b), (36) and (37). The black solid line is the numerical solution using the Direct Integration Method [26]. The initial wave surface is a Gaussian group $\zeta(x,0) = a\exp(-\frac{1}{2}x^2/L^2)\cos(k_0 x)$ with $k_0 L = 1$The focusing occurs at $t = 0$.

For a particular propagation direction θ it is sufficient that $\delta(\mathbf{k}) \ll 1$ for all significant values of k. The maximum absolute value of δ_α is at $k = \alpha/2$ where

$$\delta_{\alpha,\max} = |U_{x0}|\sqrt{\alpha/8g}. \tag{34}$$

Note that the global maximum of δ_α does not depend on the lengthscale L, i.e., $\delta_{\max} \ll 1$ guarantees the accuracy of weak-shear theory independently of the size and shape of the wave group at focus, as should be expected. However, note that this is a sufficient, not a necessary condition: if αL is much greater or smaller than unity, δ_α could remain far smaller than its maximal value for all k which contribute significantly.

We note in passing the corrensponddence with the assumption in Stewart & Joy's theory of weak current compared to the phase velocity; at $k = \alpha/2$ the condition $\delta_{\max} \ll 1$ can be written $U_{x0}/2c \ll 1$ since the phase velocity

is approximately $\sqrt{2g/\alpha}$. This is a (reference system invariant) weak current assumption: the maximum difference in $U_{x0}(z)$ over the water column is much smaller than twice the phase velocity.

The weak-shear approximation, eq. (23), yields

$$\omega(k) \approx \sqrt{gk} - \frac{U_{x0}\alpha k}{2k+\alpha}; \tag{35a}$$

$$A_{\mathrm{sp}} = \xi = \frac{1}{2}\sqrt{\frac{g}{k_{\mathrm{sp}}}} - \frac{U_{x0}\alpha^2}{(2k_{\mathrm{sp}}+\alpha)^2}; \tag{35b}$$

$$B_{\mathrm{sp}} = -\frac{1}{4k_{\mathrm{sp}}}\sqrt{\frac{g}{k_{\mathrm{sp}}}} + \frac{4U_{x0}\alpha^2}{(2k_{\mathrm{sp}}+\alpha)^3} = -\frac{\xi}{2k_{\mathrm{sp}}} - \frac{U_{x0}\alpha^2(\alpha-6k_{\mathrm{sp}})}{2k_{\mathrm{sp}}(2k_{\mathrm{sp}}+\alpha)^3}. \tag{35c}$$

We wish to solve (35b) with respect to k_{sp}. The assumption behind the weak-shear approximation is that $\delta \ll 1$ as defined in Eq. (20). In this spirit we write $\alpha U_{0k} \to \gamma\alpha U_{0k}$ with γ a "smallness" parameter for bookkeeping we will eventually take to 1. We expand $k_{\mathrm{sp}} = k_{\mathrm{sp}}^{(0)} + \gamma k_{\mathrm{sp}}^{(1)}$ and solve (35b) in orders of γ and insert into (35c) to obtain

$$k_{\mathrm{sp}} = \frac{g}{4\xi^2} - \frac{2gU_{x0}\alpha^2\xi}{(g+2\alpha\xi^2)^2} + \mathcal{O}(\gamma^2); \tag{36}$$

$$B_{\mathrm{sp}}(\xi) = -\frac{2\xi^3}{g} - \frac{8U_{x0}\alpha^2\xi^6(g-6\alpha\xi^2)}{g(g+2\alpha\xi^2)^3} + \mathcal{O}(\gamma^2). \tag{37}$$

The frequency in the weak-shear stationary phase approximation is found by inserting (36) into (35a) and retaining terms to $\mathcal{O}(\gamma)$,

$$\omega_{\mathrm{sp}} = \frac{g}{2\xi} - \frac{U_{x0}g\alpha(g+6\alpha\xi^2)}{2(g+2\alpha\xi^2)^2} + \mathcal{O}(\gamma^2), \tag{38}$$

while the applicability of weak-shear theory is well indicated by the Froude-shear number at the stationary point,

$$\delta_{\alpha,\mathrm{sp}} = \frac{\alpha\xi U_{x0}}{g+2\xi^2\alpha} + \mathcal{O}(\gamma^2) \tag{39}$$

which has its maximum at $\xi = \sqrt{g/2\alpha}$ where the result (34) is regained.

We test the stationary phase surface elevation solution in figure 4. The red line indicates the arbitrary-accuracy numerical solution using the method of reference [26], whereas the black is the weak-shear stationary phase solution, found by inserting (38) and (37) into equation (32). We observe a very slight phase shift over time because the frequency ω_{sp} is only approximate, whereas the 'exact' and approximate envelope of the group are virtually indistinguishable.

3.2.2 Stationary phase approximation for linear shear

In the special case of linear shear, an explicit formula is readily derived. Rather than use Eq. (32) we substitute $\varpi = \sqrt{gk + \sigma^2}$ into the dispersion relation (14), $\omega = \omega_\sigma = \varpi - \sigma$, from which it follows that $k(\varpi) = (\varpi^2 - \sigma^2)/g$; $\mathrm{d}k = (2\varpi/g)\mathrm{d}\varpi$, and according to equation (12) $\zeta(x,t)$ is,

$$\begin{aligned}\zeta(x,t) =& 2\,\mathrm{Re}\int_0^\infty \frac{\mathrm{d}k}{2\pi}\tilde{\zeta}_0(k)\mathrm{e}^{ikx-i\omega_\sigma t}\\ =& \frac{2}{\pi g}\,\mathrm{Re}\left[\mathrm{e}^{-ix\sigma^2 g+i\sigma t}\int_{|\sigma|}^\infty \mathrm{d}\varpi\,\varpi\tilde{\zeta}_0(k(\varpi))\mathrm{e}^{ix\varpi^2/g-i\varpi t}\right].\end{aligned} \tag{40}$$

Formally we write the exponent as $it\phi(\varpi)$ with $\phi(\varpi) = \varpi^2 x/gt - \varpi$, and consider the asymptote $t \to \infty$ while assuming $x/t \sim \mathcal{O}(1)$. The stationary phase $\varpi = \varpi_{\mathrm{sp}}$ is

$$\phi'(\varpi_{\mathrm{sp}}) = \left(\frac{2x}{gt}\varpi_{\mathrm{sp}} - 1\right)\Big|_{\varpi=\varpi_{\mathrm{sp}}} = 0, \tag{41}$$

or, in other words, $\varpi_{\mathrm{sp}} = gt/2x$. (Introduction of the symbol $\xi = x/t$ is not equally handy as in the previous section, and we retain x and t here.) With the stationary phase approximation the integral is (e.g., §6.5 of [23])

$$\int_{|\sigma|}^\infty \mathrm{d}\varpi\,\varpi\tilde{\zeta}_0(k(\varpi))\mathrm{e}^{ix\varpi^2/g-i\varpi t} \approx \sqrt{\frac{\pi g}{|x|}}\frac{t\tilde{\zeta}_0(k_{\mathrm{sp}})}{2x}\exp i\left[-\frac{gt^2}{4x}+\frac{\pi}{4}\mathrm{Sg}(x)\right]\Theta(k_{\mathrm{sp}}) \tag{42}$$

with

$$k_{\mathrm{sp}} = \frac{\varpi_{\mathrm{sp}}^2 - \sigma^2}{g} = \frac{gt^2}{4x^2} - \frac{\sigma^2}{g}. \tag{43}$$

There is no stationary point unless $t/2x > |\sigma|$, hence the unit step function Θ. Thus, taking the real part, the stationary phase approximation to $\zeta(x,t)$ is

$$\zeta(x,t) \approx \sqrt{\frac{g}{\pi|x|}}\frac{t}{x}\mathrm{Re}\left\{\tilde{\zeta}_0(k_{\mathrm{sp}})\exp i\left[-\frac{\sigma^2 x}{g}-\frac{gt^2}{4x}+\sigma t+\frac{\pi}{4}\mathrm{Sg}(x)\right]\right\}\Theta(k_{\mathrm{sp}}). \tag{44}$$

The approximation is only nonzero when x and t are either both negative or both positive, as is reasonable since we have assumed propagation towards positive x. In the symmetrical case where $\zeta(x,0) = \zeta(-x,0)$, $\tilde{\zeta}_0(k)$ is real and the exponential becomes a cosine.

3.3 Waves focusing to δ-function singularity

Assuming the wave form at focus is a Dirac δ function is the most extreme form of focusing. As is conventional, we overlook the obvious fact that linear theory cannot describe such a wave packet close to its maximum, and regard

the solution some time before and after focusing. The case is particular in the sense that the wave shape at focus has no intrinsic length scale. We write the elevation at focus with the delta function in the limit form [e.g., 27, §7.2]

$$\zeta(x,0) = a\delta(x/L) = \lim_{\mu\to 0^+} \frac{a}{\pi}\frac{\mu}{x^2/L^2+\mu^2} \tag{45}$$

where L is some arbitrary, finite lengthscale for dimensional reasons (in later sections it will play the role of characteristic width of the wave packet at focus). Its obtains physical meaning is only when this singular model flow is compared to whatever real flow it models. The Fourier transform is

$$\tilde{\zeta}_0(k) = aL \lim_{\mu\to 0^+} e^{-\mu L|k|}. \tag{46}$$

Using (12) we have

$$\zeta(x,t) = 2aL \lim_{\mu\to 0^+} \int_0^\infty \frac{\mathrm{d}k}{2\pi} \cos[kx-\omega(k)t]e^{-\mu Lk}. \tag{47}$$

The role of μ is to render the integral well defined.

For an integral with rapidly oscillating integrand of form

$$\int \mathrm{d}q f(q) e^{iX\phi(q)} \tag{48}$$

with $\phi(q) \sim \mathcal{O}(1)$, the stationary phase approximation is accurate for $X \gg 1$ assuming $f(q)$ is significant for $q \sim \mathcal{O}(1)$. Substituting $q = \mu k$ into (47), we observe that $X = x/\mu$, which is very large for any nonzero x. Thus the stationary phase approximation should be sufficiently accurate everywhere, for practical purposes.

From equation (44) the stationary phase approximation for linear shear is

$$\zeta(x,t) = aL\sqrt{\frac{g}{\pi|x|}}\frac{t}{x}\cos\left[\frac{\sigma^2 x}{g}+\frac{gt^2}{4x}-\sigma t-\frac{\pi}{4}\mathrm{Sg}(x)\right]\Theta\left(\frac{gt^2}{2x}-|\sigma|t\right). \tag{49}$$

Corresponding expressions for $\zeta(x,t)$ on other shear currents, including the special case of an exponential currents, are obtained by inserting $\tilde{\zeta}_{\mathrm{sp}} = aL$ into the results in sections 3.2.

The surface elevation for a linear wave focusing towards a δ-function singularity is shown in Fig. 5. Lines show a direct calculation of integral (47) with the integration path rotated slightly into the complex k plane (closed with a non-contributing arc at infinity), ensuring exponential convergence. Let $\tilde{\sigma} = \sigma T_{\mathrm{ref}}$ and $\tilde{t} = t/T_{\mathrm{ref}}$ with reference time $T_{\mathrm{ref}} = \sqrt{L/g}$. Three different shear strengths are shown: $\tilde{\sigma} = -0.5, 0$ and 0.5 with reference time The circular markers are the values obtained using equation (49); these are indistinguishable from the exact integral in all cases. As discussed in connection

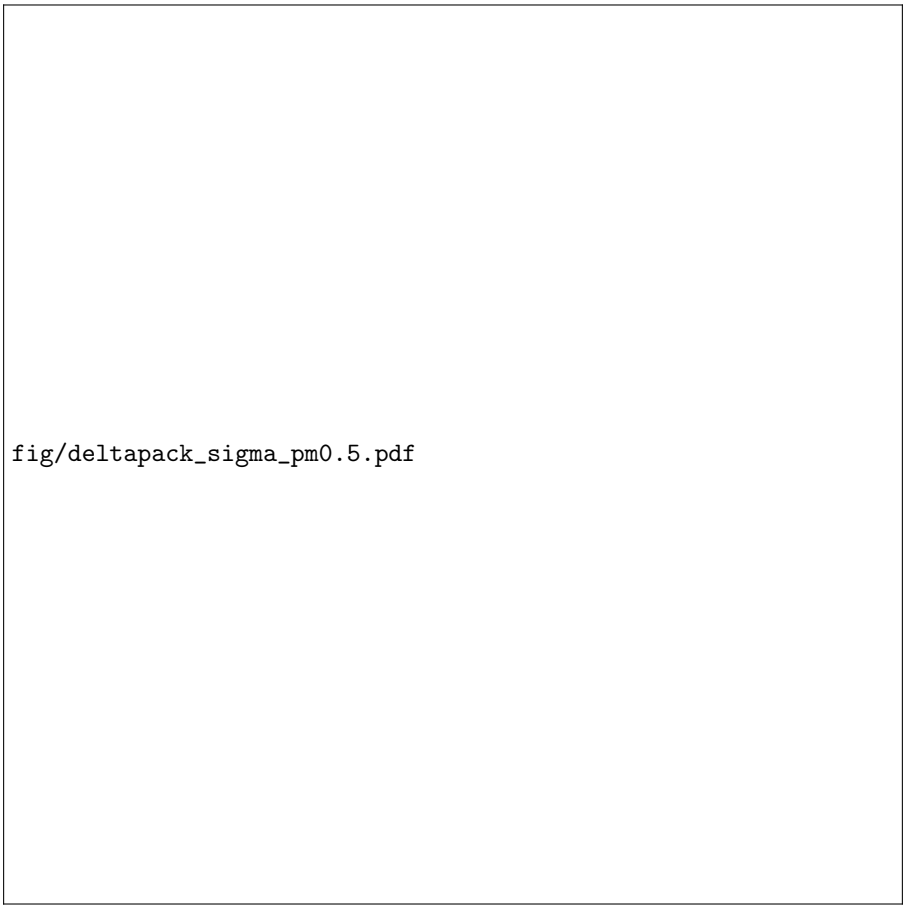

Fig. 5 Surface elevation ζ/a (x in units of L, t in units of $T_{\mathrm{ref}} = \sqrt{L/g}$) for a wave group focusing to a δ-function singularity on a linear shear current. a) $t = -25\,T_{\mathrm{ref}}$, b) $t = -5\,T_{\mathrm{ref}}$. Three different shear strengths: $T_{\mathrm{ref}}\sigma = -0.5$ (blue, solid), $T_{\mathrm{ref}}\sigma = 0.5$ (black, dashed), and $T_{\mathrm{ref}}\sigma = 0$ (red, dotted); circular markers show the stationary phase approximation (49).

with equation (44), the cases $\tilde{\sigma} = -0.5$ and 0.5 are nearly indistinguishable at $\tilde{t} = -25$, but differences manifest at the later time $\tilde{t} = -5$.

In stark contrast, the behaviour of the wave phase for case $\tilde{\sigma} = 0$ is always quite distinct from the others, as should be obvious from inspection of the argument of the cosine in Eq. (49), where the term $\sigma^2 x/g$ is highly significant when $t/x \sim \sigma/g$. This observation has consequences for creating a focusing wave in a laboratory with a shear current.

An approximate solution in the shallow-water limit, which generalises results in Refs. [25, 28], is found in appendix A.2.

3.4 Long wave group with Gaussian envelope

We next consider a group with Gaussian envelope of characteristic length L and carrier wave number $k_0 > 0$, i.e.,

$$\zeta(x,0) = ae^{-x^2/2L^2}\cos(k_0 x). \tag{50}$$

We allow the shear current $U(z)$ in equation (1) to be arbitrary and assume $\omega(k)$ and its first and second derivatives are known. Note that $k_0 L$ now acts as a bandwidth parameter: The higher $k_0 L$, the narrower the bandwidth: $k_0 L$ is approximately the number of wavelengths of the carrier wave within the group. We will assume in derivations that the group is long (i.e., narrowband), $k_0 L \gg 1$, yet we will see in the following that narrowband (long-group) approximations are excellent for many practical purposes already at $k_0 L = 3$ - 5 which would not in most cases be considered a 'long' group.

Taking the Fourier transform of the Gaussian group we obtain with equation (11)

$$\zeta(x,t) = \frac{aL}{\sqrt{2\pi}}\int_0^\infty \mathrm{d}k\left[e^{-\frac{1}{2}(k-k_0)^2L^2} + e^{-\frac{1}{2}(k+k_0)^2L^2}\right]\cos[kx-\omega(k)t]. \tag{51}$$

When $k_0 L \gg 1$, only the first term in the brackets makes a significant contribution, so, ignoring a term of order $\exp(-\frac{1}{2}k_0^2L^2)$, we may simplify (51) to

$$\zeta(x,t) \approx \frac{aL}{\sqrt{2\pi}}\int_0^\infty \mathrm{d}k\, e^{-\frac{1}{2}(k-k_0)^2L^2}\cos[kx-\omega(k)t]. \tag{52}$$

This simplification becomes suspect for $k_0 L \lesssim 3$, depending on the required level of accuracy.

This is the Gaussian group in the sense of [15], prescribing the spatial shape of the wave at focus, slightly different from the definition used in, e.g., [29, 30] where the time series of the wave elevation is specified in the time domain.

The integral (52) gets its significant contributions from near $k = k_0$. The longer the group, i.e., the more periods of the carrier wave it contains, the more focused the integral is around this value. We thus assume the group width L is much larger than a wavelength, i.e., $k_0 L \gg 1$. Following [15] we expand the dispersion relation in a Taylor series around $k = k_0$,

$$\omega(k) = \omega(k_0) + A_0(k-k_0) + \tfrac{1}{2}B_0(k-k_0)^2 + \ldots \tag{53}$$

where

$$A_0 = \left.\frac{\mathrm{d}\omega}{\mathrm{d}k}\right|_{k=k_0}; \quad B_0 = \left.\frac{\mathrm{d}^2\omega}{\mathrm{d}k^2}\right|_{k=k_0} \tag{54}$$

are found from the dispersion relation, either analytically or numerically using, e.g., the Direct Integration Method [26].

Since $k_0 L$ is large the resulting integral is of Laplace type and is approximated as such (see, e.g., § 6.4 of [23]) whereby ζ tends asymptotically to

$$\frac{\zeta(x,t)}{a} \approx \frac{L}{\sqrt{2\pi}}\mathrm{Re}\left\{ e^{ik_0x - i\omega(k_0)t} \int_{-\infty}^{\infty} \mathrm{d}q\, e^{-\frac{1}{2}(L^2+iB_0t)q^2 + iq(x-A_0t)} \right\} \tag{55a}$$

$$= \mathrm{Re}\left\{ \frac{L}{\sqrt{L^2+iB_0t}} \exp\left[ik_0x - i\omega(k_0)t - \frac{(x-A_0t)^2}{2(L^2+iB_0t)} \right] \right\} \tag{55b}$$

with $q = k - k_0$. Taking the real part readily yields

$$\frac{\zeta(x,t)}{a} \approx \left(\frac{L^4}{L^4 + B_0^2t^2} \right)^{\frac{1}{4}} \exp\left[-\frac{L^2(x-A_0t)^2}{2(L^4+B_0^2t^2)} \right]$$
$$\times \cos\left[k_0x - \omega(k_0)t - \frac{1}{2}\arctan\left(\frac{B_0t}{L^2}\right) + \frac{(x-A_0t)^2B_0t}{2(L^4+B_0^2t^2)} \right]. \tag{56}$$

This is the very general result of Ref. [15]. The effect of currents (and other factors affecting the dispersion, such as finite depth) is only to modify the expressions for A_0 and B_0 through the more general dispersion relation. For gravity waves, A_0 is typically positive and B_0 negative. In the cases we consider, the approximation (56) is reasonable already at $k_0L \sim 3$, adequate for many purposes.

3.4.1 Linear shear

Turning to our special case of constant shear and deep water, A_0 and B_0 are easily found from Eq. (14) and may be instructively written in terms of a shear-modified wave number (see eq. (15))

$$\varkappa_0 = k_0 + \sigma^2/g \tag{57}$$

as

$$A_{0,\mathrm{lin.}} = \tfrac{1}{2}c_0(\varkappa_0); \quad B_{0,\mathrm{lin.}} = -\tfrac{1}{4}c_0(\varkappa_0)/\varkappa_0 \tag{58}$$

with $c_0(k) = \sqrt{g/k}$ as usual. Insertion into (56) gives the approximation of $\zeta(x,t)$ for a long Gaussian focusing group. Expressions for general water depth are derived in A.3.

Figure 6 compares the approximation (56) to the exact linear solution (52) for Gaussian groups of two different lengths and strong following and opposing shear, $\tilde{\sigma} = -0.5$ and $\tilde{\sigma} = 0.5$ for the left and right group on each horizontal line, respectively. In Fig. 6b a moderately long packet ($k_0L = 10$) is considered, and the approximation (56) is excellent in all cases, out to having propagated 50 times the initial group width. Surprisingly, Fig. 6a shows how even for a short package $k_0L = 3$ performs reasonably well especially in the central region of the group. In accordance with our discussion in Section 3.1, the development of the envelopes in time is indistinguishable for the two opposite, strong shear currents, making still images of surface elevations such as these qualitatively indistinguishable.

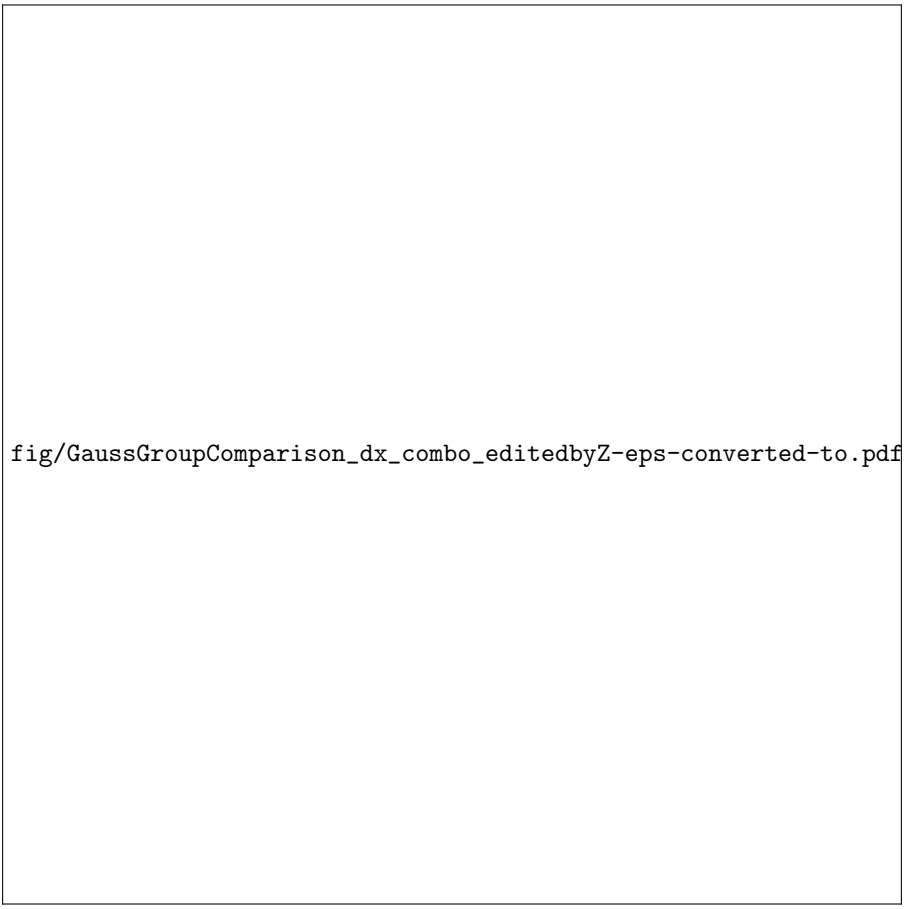

Fig. 6 Comparison of exact and approximate linear solution for a defocusing Gaussian wave group on linear currents with $\tilde{\sigma} = -0.5$ and $\tilde{\sigma} = 0.5$ for the packets to the left and right on each horizontal line, respectively, as a function of x measured in number of "widths" L of the Gaussian envelope at focus. The first time (bottommost line of graphs) is at focus, whereupon defocusing is illustrated with time increasing from bottom to top in each panel by intervals $\Delta T = 10L/c_g$ with $c_g(k_0) = A_{0,\text{lin.}}$ from Eq. (58) (i.e., the group travels 10 times the 'envelope width' between subsequent times). Thin black line: full linear solution (52), thick red graph: approximation (56). a) Short group, $k_0 L = 3$, focusing at $x = 0$ and $x = 60L$. b) Long group, $k_0 L = 10$ focusing at $x = 0$ and $x = 30L$, respectively.

3.4.2 Arbitrary current with weak shear

The first two derivatives of $\sigma_\delta(k)$ from equation (22) are

$$\sigma'_\delta(k) = \int_{-\infty}^{0} \mathrm{d}z\,(1+2kz)U'_x(z)\mathrm{e}^{2kz}; \tag{59a}$$

$$\sigma''_\delta(k) = 4\int_{-\infty}^{0} \mathrm{d}z\,z(1+kz)U'_x(z)\mathrm{e}^{2kz}, \tag{59b}$$

from which we obtain, by insertion into Eq. (54), the coefficients A_0 and B_0 for use in equation (56)

$$A_{0\delta} = \tfrac{1}{2}c_0(k_0) - \sigma'_{\delta 0}(k_0); \qquad B_{0\delta} = -\tfrac{1}{4}c_0(k_0)/k_0 - \sigma''_{\delta 0}(k_0). \tag{60}$$

Comparison with Eq. (58) shows that the first term on the right-hand sides of Eq. (60) are the no-shear expressions, and the remaining terms are corrections due to the weakly sheared current.

The quantities $\sigma_\delta, \sigma'_\delta$ and σ''_δ can be written in closed form for a number of different profiles $U_x(z)$ including the linear current (a special case where the weak-shear theory does not perform particularly well [24]) and the exponential which we consider next.

Note in passing that with a partial integration of (22) we may write

$$\sigma_\delta(k) = \tfrac{1}{2}U'_x(0) - \tfrac{1}{2}\int_{-\infty}^{0} \mathrm{d}z\, U''_x(z)\mathrm{e}^{2kz}; \tag{61a}$$

$$\sigma'_\delta(k) = -\int_{-\infty}^{0} \mathrm{d}z\, zU''_x(z)\mathrm{e}^{2kz}; \tag{61b}$$

$$\sigma''_\delta(k) = -2\int_{-\infty}^{0} \mathrm{d}z\, z^2U''_x(z)\mathrm{e}^{2kz}; \tag{61c}$$

in other words, σ_δ represents the first-order correction to the wave-averaged shear compared to the surface shear because $U_x(z)$ has nonzero curvature. This is an indication why the weak–curvature theory in section 2.4.2 becomes exact for the linear current which has $U''(z) = 0$, and also why the linear current is a special case where weak–shear theory does not perform very well: the shear correction to A_0 and B_0 for linear shear in equation (58) (which is exact for the linear–current case) is symmetrical under $\sigma \to -\sigma$, but (60) does not have this symmetry under $\sigma_\delta \to -\sigma_\delta$. Another way of putting it is that when shear-current corrections in the surface-following system may be treated perturbatively, the first-order correction to the phase velocity is due to mean shear, but for the group velocity it is due to mean curvature. When the curvature vanishes, however, the leading group-velocity correction becomes second order in the average shear. For further discussions, see [20].

3.4.3 Exponential shear. Weak-shear approximation vs numerical solution

As a particular example consider the exponential current (19). We will see that a number of useful approximate expressions can be found assuming weak shear and exponential current. Note that even the Columbia River delta shear current, considered to be a very strongly sheared current in this context [31], the weak-shear approximation is sufficient for most practical purposes as we detail in section 3.4.4.

We find $A_0 = A_{0\alpha}$ and $B_0 = B_{0\alpha}$ with

$$A_{0\alpha} = \tfrac{1}{2}c_0(k_0) - \frac{U_{x0}\alpha^2}{(2k_0+\alpha)^2}; \qquad B_{0\alpha} = -\frac{c_0(k_0)}{4k_0} + \frac{4U_{x0}\alpha^2}{(2k_0+\alpha)^3}. \tag{62}$$

In figure 7 the approximate solution (56) with coefficients (62) inserted is compared with the 'exact' numerical solution of the linear-wave initial value problem. It is striking that although the derivation assumes $k_0L \gg 1$, the approximation is reasonable already for $k_0L = 3$. Moreover, the shear is here not extremely weak; from equation (33) we find that for maximally opposing shear ($\theta = 0$), $\delta(k_0) = 0.10$ and $\delta(k_0) = 0.07$ for $k_0L = 3$ and 10, respectively, the former of which is slightly higher than that for the Columbia River scenario we consider in sections 3.4.4 and 4.5.1. This demonstrates the wide applicability of the simple closed-form approximation, equations (56) and (62). A slight phase shift with propagation is observed in both cases in figure 7 due to the approximate dispersion relation, from equations (23) and (33). In both cases in figure 7 the envelope is excellently approximated; we quantify this in figure 8 where the decaying height of the defocusing wave group is plotted. Even for $k_0 = 2$ the agreement is reasonable although this can in no way be called a 'narrowband' wavegroup.

3.4.4 Measured current profiles: The Columbia River estuary

The flow conditions in the estuary of the Columbia River have been much studied for a long time (e.g., [32–34]) due to its strong, and strongly sheared, tidal current, severe wave climate and high shipping traffic. It is also a much used case for studies of waves interacting with sheared currents in various contexts (examples include [24, 26, 35–37]).

In their study of the Columbia River delta, Zippel & Thomson [38] (ZT) measured simultaneous wave spectra and shear current profiles in the delta of the Columbia River. An even more strongly sheared current is found among the measurements of Kilcher & Nash (KN) from the same area [39] (another set of measurements is described and used in refs [33, 35, 37]). Their respective current profiles are shown in figure 9. In section 4.5.1 we also make use of the measured wave spectrum in reference [38], while here we shall use a model wave group which at focus is slightly more narrowband than the one measured; this would represent the situation where only the part of the spectrum near the peak is involved in the focusing, the remainder forming a small-amplitude random-phase background which we presently ignore.

The velocity profiles shown were shifted to the reference frame following the mean (Eulerian) surface velocity and fitted to an exponential profile $U(z) = U_0[\exp(\alpha z) - 1]$ (see figure 9c) which gives $U_0 = 1.6\,\mathrm{m/s}$, $\alpha = 0.26\,\mathrm{m}^{-1}$ for current ZT and $U_0 = 1.4\,\mathrm{m/s}$, $\alpha = 0.39\,\mathrm{m}^{-1}$ for current KN.

To study an example of a focusing group we choose reasonable values for a dispersively focusing wave group in this location — see also section 4.5.1:

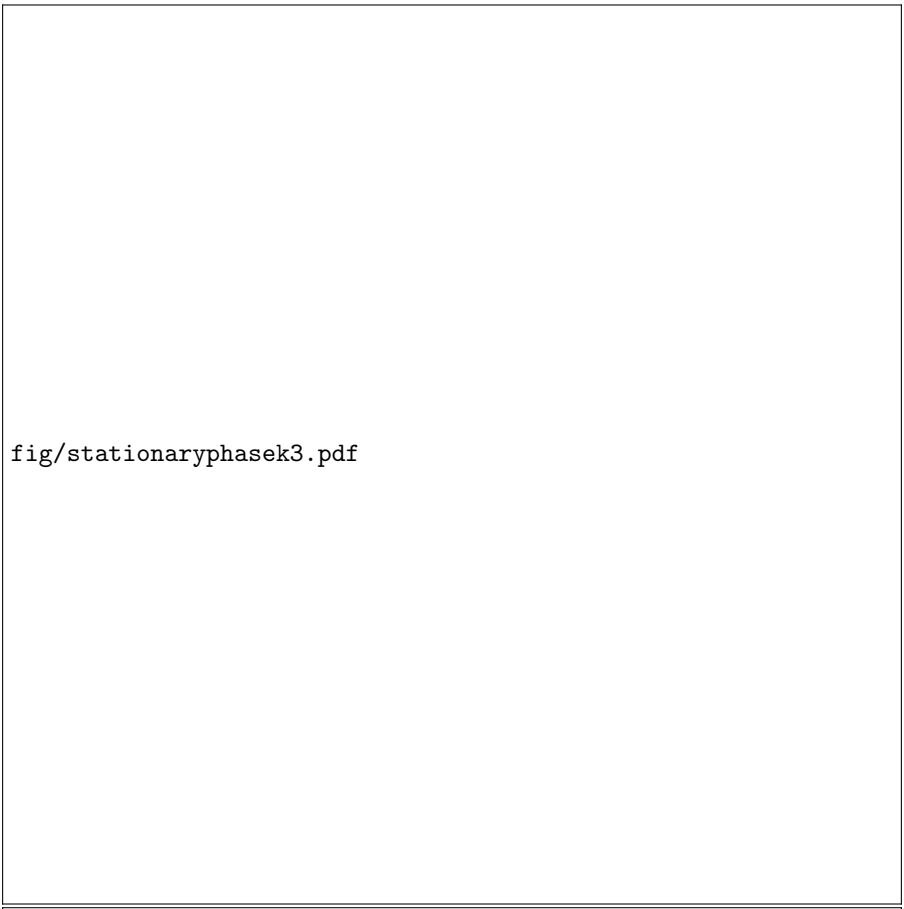
fig/stationaryphasek3.pdf


fig/stationaryphasek10.pdf

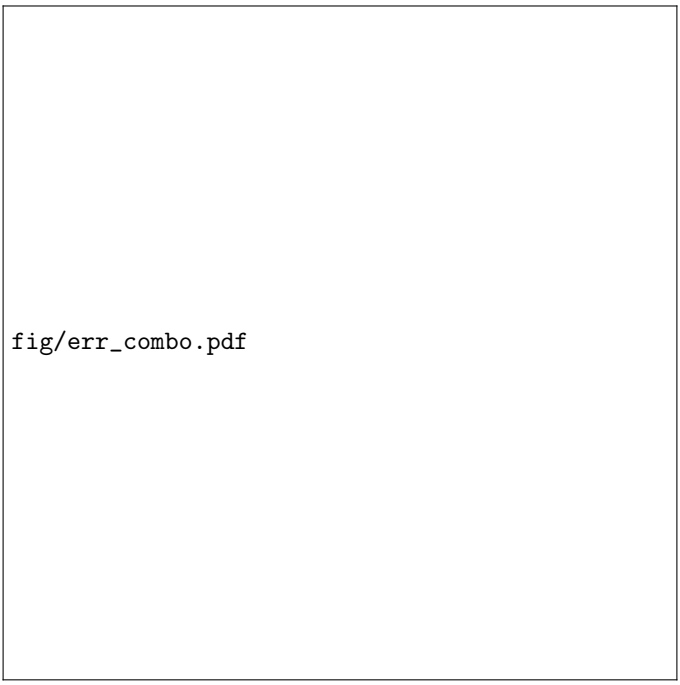

Fig. 8 The decay of envelope amplitude for increasing wave group length k_0L (decreasing spectral bandwidth) on the same exponential shear current as in figure 7. Each point is calculated as the maximum modulus of the Hilbert transform of the analytic surface elevation. Red solid lines: narrow-band weak-shear approximation. Black dash-dot lines: 'exact' numerical solution.

$k_0 = 0.15\,\mathrm{rad/m}$, $L = 20\,\mathrm{m}$, which gives $k_0L = 3.0$. We choose for our example the average of the two values for U_0 and α, respectively.

It is worth pointing out at this stage that these parameters give a shear Froude number of $\delta_{0\alpha} = 0.11$ (KN) and 0.080 (ZT), respectively, when inserted into equation (33) ($\delta_{0\alpha} = 0.090$ with the chosen model parameters); in other words, even though the Columbia River current is frequently used as an example of a very strongly sheared current where the effect of shear on the waves is highly significant, we can safely employ weak-shear theory with errors no greater than a few percent, less than those from typical measurement uncertainty from field measurements. Moreover, although $k_0L = 3$ is not what one would refer to as a narrowband wave group, we see from Fig. 7 that narrow-band weak-shear theory gives a more than adequate approximation of the surface. Thus we may confidently approximate $\zeta(x,t)$ with the approximate formula (56) with coefficients (62) inserted.

With the mentioned approximation we plot a focusing and defocusing wave group representative of the Columbia River flow conditions, in figure 10. Albeit less extreme than for the model linear current, the trend is once again clear: in the case of opposing shear (the focusing group propagates 'downstream' in the river, in an earth-fixed system) the crests and troughs focus and defocus more

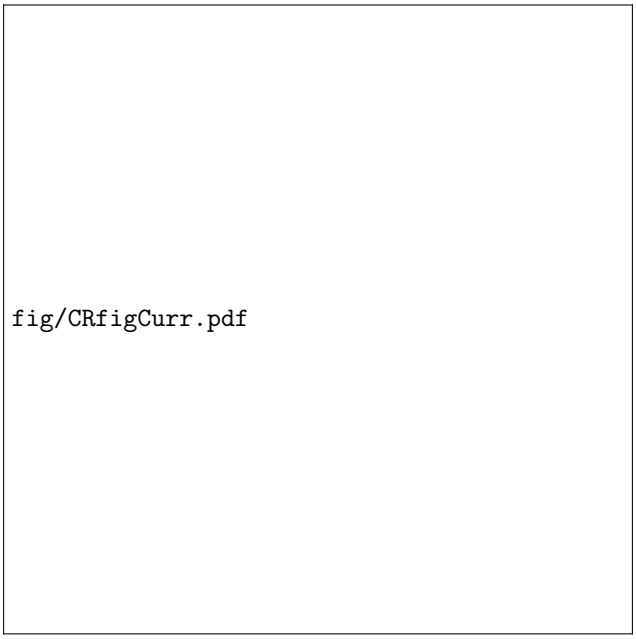

Fig. 9 Shear current profiles of the Columbia River delta current. Measured data by Zippel & Thomson (blue dots) and Kilcher & Nash (red crosses), the lines are exponential functions of form (19) fitted to the data.

gently than for the case of following shear ('upstream') where individual crests and troughs within the group move faster and live shorter. The corresponding increase in orbital velocities in the latter case is considered and quantified in section 4.5.1. Once again we notice that the group envelope, represented by the change in maximum group height with time, varies modestly.

3.4.5 Arbitrary current with strong shear

Insering dispersion relation (24) into formula (54) now gives the coefficients A_0 and B_0 for strong shear in the strong shear, weak curvature approximation (SSWCA) of Ellingsen & Li [20],

$$A_{0,\mathrm{EL}} = \tfrac{1}{2}c_0(\varkappa_{\delta 0})(1 + 2\sigma_{\delta 0}\sigma'_{\delta 0}/g) - \sigma'_{\delta 0} \tag{63a}$$

$$B_{0,\mathrm{EL}} = -\frac{(g + 2\sigma_{\delta 0}\sigma'_{\delta 0})^2}{4\omega_0(\varkappa_{\delta 0})^3} + \frac{\sigma'^2_{\delta 0} + \sigma_{\delta 0}\sigma''_{\delta 0}}{\omega_0(\varkappa_{\delta 0})} - \sigma''_{\delta 0}, \tag{63b}$$

where we use the shorthand $\varkappa_{\delta 0} = \varkappa_\delta(k_0)$ and $\omega_0(\varkappa_{\delta 0}) = \sqrt{g\varkappa_{\delta 0}} = \varkappa_{\delta 0}c_0(\varkappa_{\delta 0})$; $\varkappa_\delta$ was defined in equation (25). If the Froude-shear number δ is small we obtain (60) to leading order, while assuming linear shear ($\varkappa_\delta(k) \to \varkappa$, and $\sigma'_\delta = \sigma''_\delta = 0$) yields expressions (58). The SSWCA should replace the weak-shear approximation when the shear as seen by the significant waves as

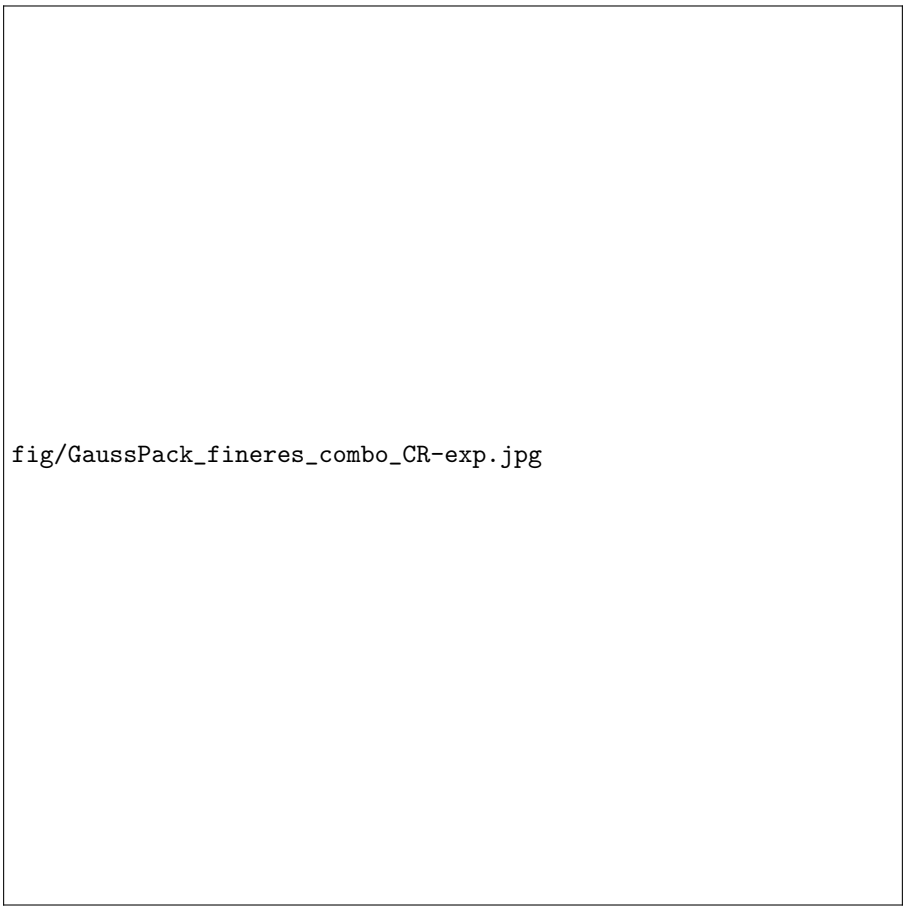

Fig. 10 Same illustration as in figure 2, but with an exponential current representative of the Columbia River, shown in figure 9; see main text for further details. The exponential profile (19) is used with $k_0 L = 3$, $\alpha L = 6.5$ and $U_0 = 0.107\, U_{\rm ref}$ with $\theta = 0, \pi/2$ and π (top to bottom). The nondimensional time $\tilde{t}$ runs from from -50 to 50 in steps of 0.4. The dashed lines are plots of the maximum height, $\pm L(L^4 + B_{0\alpha}^2 t_g(x)^2)^{-1/4}$ with $t_g(x) = x/A_{0\alpha}$.

extremely strong (by oceanographic standards), i.e., when δ is not small compared to 1, and/or the current shear appears close to constant with depth. For the exponential current representative of the Columbia River, figure 9, using expressions (63) instead of (62) gives practically identical results. Deriving explicit formulae for $A_{0,\rm EL}$ and $A_{0,\rm EL}$ with the exponential current (19) is straightforward, but the resulting expressions are sufficiently bulky that we do not quote them here. Several realistic situations where the weak-shear theory is insufficient are mentioned and discussed in reference [20], although these are not currents which occur in ocean or coastal waters.

4 Wave kinematics and orbital velocities

We proceed now to considering the shear-affected wave orbital motion. We consider three cases, a weakly sheared current in the approximation of [14] (see sections 2.4.1 and 3.4.2), and two cases where an exact solution to the linear problem exists: a current with constant shear and with exponential shear.

Taking a step back to the more general formalism of section 2, we set $\mathbf{k} = \{k_x, 0\}$ (k_x once again takes either sign) and write the orbital velocities of a linear plane wave as

$$\begin{bmatrix} u(x,z,t) \\ v(x,z,t) \\ w(x,z,t) \end{bmatrix} = \mathrm{Re} \int_0^\infty \frac{\mathrm{d}k}{2\pi} \begin{bmatrix} \tilde{u}(z,t;\ k) \\ \tilde{v}(z,t;\ k) \\ \tilde{w}(z,t;\ k) \end{bmatrix} e^{ikx} + \text{c.c.} \tag{64}$$

where as before we used that if some function $\varphi(x)$ is real, its Fourier transform satisfies $\tilde{\varphi}(-k_x) = \tilde{\varphi}^*(k_x)$ to only retain positive values of k. Solving the 3-dimensional, linearised Euler equation in Fourier form produces the well-known Rayleigh equation (e.g. [16, 40])

$$\left[\partial_z^2 - k^2 + \frac{\mathbf{k}\cdot\mathbf{U}''(z)}{\omega - \mathbf{k}\cdot\mathbf{U}(z)}\right] \tilde{w}(z,t;\ \mathbf{k}) = 0 \tag{65}$$

(note that $k = |\mathbf{k}| = |k_x|$ here). Once w is found, the horizontal velocity components $\tilde{\mathbf{u}}_\perp = \{\tilde{u}, \tilde{v}\}$ are obtained using the general relation [26]

$$k^2(\omega - \mathbf{k}\cdot\mathbf{U})\tilde{\mathbf{u}}_\perp = i[\mathbf{k}\cdot\mathbf{U}'\tilde{w} + (\omega - \mathbf{k}\cdot\mathbf{U})\tilde{w}']\mathbf{k} - ik^2\mathbf{U}'\tilde{w}, \tag{66}$$

where the arguments of $\tilde{\mathbf{u}}_\perp(z,t;\ \mathbf{k}), \tilde{w}(z,t;\ \mathbf{k}), \mathbf{U}(z)$ and $\omega(\mathbf{k})$ are understood, and a prime denotes derivative with respect to z. Note in particular that when $\mathbf{k} = \{k, 0\}$, one finds

$$\tilde{u} = i\tilde{w}'/k; \tag{67a}$$

$$\tilde{v} = \frac{-iU_y'(z)}{\omega - kU_x(z)}\tilde{w}. \tag{67b}$$

The eigenvalues of $\omega(k)$ are real provided the denominator in (65) is not zero [41], i.e., no critical layer exists. We shall assume this to be the case, physically implying that no critical layers occur.

Equation (67b) shows how the orbital velocities are modified by the shear current also for $\theta = \pi/2$ (i.e., $\mathbf{k}\cdot\mathbf{U} = kU_x = 0$), even though the surface elevation is equal to that without current in that case (equation (3) shows that ζ is affected by the current only via the dispersion relation $\omega(\mathbf{k})$, in turn obtained as eigenvalues of the Rayleigh equation (65) which depends only on $\mathbf{k}\cdot\mathbf{U}$.)

We now define

$$\tilde{w}(z,t;\ k) = \tilde{w}(0,t;\ k)e^{kz}f(z;\ k) \tag{68}$$

with $f(0;\ k) = 1$. The function f differs from 1 when $U_x(z)$ has curvature (i.e., nonzero second derivative) [20] — see e.g., equation (82) below. Thus, from equation (67a),

$$\tilde{u}(z,t;\ k) = i\tilde{w}(0,t;\ k)e^{kz}[f(z;\ k) + f'(z;\ k)/k]. \tag{69}$$

The kinematic boundary condition gives

$$\tilde{w}(0,t;\ k) = -i\omega(k)\tilde{\zeta}_0(k)e^{-i\omega(k)t} \tag{70}$$

where we used (7), whereby we obtain the general expressions

$$w(x,z,t) = 2\,\mathrm{Im}\int_0^\infty \frac{\mathrm{d}k}{2\pi}\omega(k)\tilde{\zeta}_0(k)f(z;\ k)e^{kz}e^{i\psi(x,t;\ k)}; \tag{71a}$$

$$u(x,z,t) = 2\,\mathrm{Re}\int_0^\infty \frac{\mathrm{d}k}{2\pi}\omega(k)\tilde{\zeta}_0(k)[f(z;\ k) + f'(z;\ k)/k]e^{kz}e^{i\psi(k)t}; \tag{71b}$$

$$v(x,z,t) = -\,2\,\mathrm{Re}\int_0^\infty \frac{\mathrm{d}k}{2\pi}\frac{\omega(k)U_y'(z)}{\omega(k) - kU_x(z)}\tilde{\zeta}_0(k)f(z;\ k)e^{kz}e^{i\psi(k)t}. \tag{71c}$$

We define the surface velocity amplification as the ratio of the horizontal orbital velocity at the (linearised) surface at the point of focus, $u(0,0,0)$, with vs without shear;

$$\mathrm{amp}_0 = \frac{\mathrm{Re}\int_0^\infty \mathrm{d}k\,\omega(k)\tilde{\zeta}_0(k)[1 + f'(0;\ k)/k]}{\mathrm{Re}\int_0^\infty \mathrm{d}k\,\omega_0(k)\tilde{\zeta}_0(k)} \tag{72}$$

with $\omega_0(k) = \sqrt{gk}$ as usual, and noting that $f(z;\ k) \to 1$ without shear.

In the presence of following shear where $U_x'(z)$ is primarily positive, the maximum of the horizontal velocity at focus $u(0,z,0)$ can lie below the surface. In this case we define a maximum amplification

$$\mathrm{amp}_{\max} = \max_z\left\{\frac{u(0,z,0)}{u_0(0,0,0)}\right\}, \tag{73}$$

where u_0 is the horizontal velocity of the no-current case.

4.1 Long Gaussian group (narrow-band)

Assume now as in section 3.4 the initial shape $\tilde{\zeta}_0(k)/aL = \sqrt{\pi/2}\exp[-\frac{1}{2}(k - k_0)^2L^2]$ with $k_0L \gg 1$. We may restrict ourselves to the upper range of the water column $|z| \ll k_0L^2$, which is no significant limitation since velocities, which decay exponentially as $\exp(k_0z)$, are negligible when $|z| \sim k_0L^2 \gg L$. The Laplace integral approximation becomes identical as in in section 3.4 with

expansion around $k = k_0$, giving the orbital velocities as the real part of

$$u \approx \frac{ac(k_0)L}{\sqrt{L^2 + iB_0t}} \exp\left[ik_0x - i\omega(k_0)t - \frac{(x - A_0t)^2}{2(L^2 + iB_0t)}\right] \frac{\mathrm{d}}{\mathrm{d}z}\left[f(z;\ k_0)e^{k_0z}\right]; \tag{74a}$$

$$v \approx -\frac{ac(k_0)k_0L}{\sqrt{L^2 + iB_0t}} \exp\left[ik_0x - i\omega(k_0)t - \frac{(x - A_0t)^2}{2(L^2 + iB_0t)}\right] \frac{U_y'(z)f(z;\ k_0)e^{k_0z}}{\omega(k_0) - k_0U_x(z)}; \tag{74b}$$

$$w \approx \frac{-iac(k_0)k_0L}{\sqrt{L^2 + iB_0t}} \exp\left[ik_0x - i\omega(k_0)t - \frac{(x - A_0t)^2}{2(L^2 + iB_0t)}\right] f(z;\ k_0)e^{k_0z}, \tag{74c}$$

with A_0, B_0 as in equation (54). We leave it to the reader write out the real part along the lines of equation (56) if desired. Correction terms of order $(x - A_0t)/k_0L$ enter far from the centre of the group at $x = A_0t$.

In the narrowband case it is opportune to also define a surface-shear number

$$\Upsilon_0 = \frac{U_x'(0)}{\omega_0(k_0)} \tag{75}$$

as well as a current strength number

$$\mathfrak{U}_0 = \frac{\max[U_x] - \min[U_x]}{c_0(k_0)}. \tag{76}$$

Here $\omega_0(k_0) = k_0c_0(k_0) = \sqrt{gk_0}$ as usual, and the functions max and min find extrema with respect to z.

In particular, for linear shear (13)

$$\Upsilon_{0,\mathrm{lin.}} = \frac{2\sigma}{\sqrt{gk_0}} = 2\,\mathrm{FS}_{\mathrm{lin.}}\cos\theta = 2\delta_{\mathrm{lin.}},$$

(σ was defined in equation (16)) whereas $\mathfrak{U}_0$ is not defined in deep water. For the exponential current profile in the Stewart & Joy weak-shear approximation, see section 4.2.1.

4.2 Wave kinematics with arbitrary, weakly sheared current

In this section we derive expressions for the orbital velocities under a focusing wave group on an arbitrary, weakly sheared current. Special cases of the final expressions, equations (83), will be simplified further in the following.

Consider a focusing wave group on a current $\mathbf{U}(z) = \{U_x, U_y\}(z)$ which is well described by the approximate theory first put forward by Stewart & Joy [14, 42] as described in section 3.4.2. This is typically a very good approximation even in strongly sheared oceanic flows (e.g. [20, 24, 26]). The orbital

velocities of a linear plane wave of wave number k of either sign in the xz-plane for such a situation have been found using assumptions of weak current [14, 42], although as discussed in section 2.4.1 these approximations are in fact valid for weakly sheared current, usefully measured via the small-shear parameter (or Froude number) $\delta(\mathbf{k})$ (see Eq. (20)).

The vertical orbital velocity to $\mathcal{O}(\delta)$ is [20, 42]

$$\tilde{w}(z,t;\ k) = \tilde{w}_0(0,t;\ k)e^{kz}\big[1-\Delta(z;\ \mathbf{k})\big]; \tag{77}$$

plus terms of $\mathcal{O}(\delta^2)$, $\tilde{w}_0$ is the vertical velocity without current (which can be related to $\tilde{\zeta}_0$ via equation (70)), and

$$\Delta(z;\ \mathbf{k}) \equiv \frac{1}{c_0}\int_{-\infty}^{z} \mathrm{d}\tilde{z}\, U_x'(\tilde{z})e^{2k(\tilde{z}-z)}. \tag{78}$$

Comparison with (20) reveals that

$$\Delta(0;\ \mathbf{k}) = \delta(\mathbf{k}), \tag{79}$$

hence $\Delta(z;\ \mathbf{k})$ is a generalisation of the small-shear Froude number $\delta(\mathbf{k})$ but with contributions only from the wave-aligned current component $U_x(z)$ at depths greater than $|z|$. (Note: Δ must not be confused with the quantity of the same name in ref [20]). Clearly $\Delta \sim \mathcal{O}(\delta)$. The dependence of Δ and δ on $\mathbf{k}$ will often be suppressed. We will need the derivative

$$\Delta'(z) = -2k\Delta(z) + U_x'(z)/c_0. \tag{80}$$

The corresponding horizontal velocities, obtained via equation (67), are

$$\tilde{u}(z,t;\ \mathbf{k}) = i\tilde{w}_0(0,t;\ k)e^{kz}\big[1+\Delta(z;\ \mathbf{k})-U_x'(z)/\omega_0\big], \tag{81a}$$

$$\tilde{v}(z,t;\ \mathbf{k}) = -\,i\tilde{w}_0(0,t;\ k)e^{kz}U_y'(z)/\omega_0 \tag{81b}$$

plus terms of order δ^2.

In the formalism of equation (68),

$$f(z;\ k) = \frac{1-\Delta(z;\ \mathbf{k})}{1-\delta(\mathbf{k})}. \tag{82}$$

The function only occurs in equations (71) in the constellation $\omega(k)f(z;\ k) = \omega_0(k)[1-\Delta(z;\ \mathbf{k})]$, using the weak-shear dispersion relation in equation (23). We shall also require the derivative $\omega f'(z) = 2k\omega_0\Delta(z;\ \mathbf{k}) - kU_x'(z)$ so that $\omega f'(0) = 2\omega_0 k\delta - kU_x'(0)$.

For a group which at $t = 0$ focuses to a shape $\zeta(x, 0)$ the velocity fields are found by insertion into (71):

$$u(x,z,t) = 2\,\mathrm{Re}\int_0^\infty \frac{\mathrm{d}k}{2\pi}\omega_0(k)\tilde{\zeta}_0(k)\left[1+\Delta(z;\,\mathbf{k})-\frac{U_x'(z)}{\omega_0}\right]e^{kz+i\psi}; \tag{83a}$$

$$v(x,z,t) = -2U_y'(z)\,\mathrm{Re}\int_0^\infty \frac{\mathrm{d}k}{2\pi}\tilde{\zeta}_0(k)e^{kz+i\psi}; \tag{83b}$$

$$w(x,z,t) = 2\,\mathrm{Im}\int_0^\infty \frac{\mathrm{d}k}{2\pi}\omega_0(k)\tilde{\zeta}_0(k)[1-\Delta(z;\,\mathbf{k})]e^{kz+i\psi}, \tag{83c}$$

plus corrections of order δ^2; here, $\psi = \psi(x, t;\, k)$.

The surface velocity amplification for an arbitrary $\mathbf{U}(z)$ satisfying $\delta(\mathbf{k}) \ll 1$ for all significantly contributing k, from equation (72), is now

$$\mathrm{amp}_{\mathrm{w.s.},0} = 1 + \frac{\int_0^\infty \mathrm{d}k\,\mathrm{Re}\{\tilde{\zeta}_0(k)\}[\omega_0\delta(\mathbf{k}) - U_x'(0)]}{\int_0^\infty \mathrm{d}k\,\omega_0\mathrm{Re}\{\tilde{\zeta}_0(k)\}}. \tag{84}$$

4.2.1 Gaussian wave group on exponential weak shear

Consider the same situation as in section 3.4.3: a Gaussian wave packet with carrier wave number k_0 considerably greater than L^{-1} i.e., the group is fairly narrowbanded. The current profile is exponential, (19) in the now familiar weak-shear approximation. A subscript 'α' will refer to the exponential current as before, and a subscript 0 means evaluation at $k = k_0$. The velocity fields are readily found from (83) by inserting $\{U_x', U_y'\}(0) = \alpha\{U_{x0}, U_{y0}\}e^{\alpha z}$ and $\Delta(z) = \Delta_\alpha(z)$ where

$$\Delta_\alpha(z) = \delta_\alpha e^{\alpha z} \tag{85}$$

with $\delta_\alpha(\mathbf{k})$ from Eq. (33). We define the shorthand

$$\mathfrak{a} \equiv \alpha/k_0. \tag{86}$$

and note that for the exponential current the definitions (75) and (76) yield

$$\mathfrak{U}_{0\alpha} = \frac{U_{x0}}{c_0(k_0)}; \quad \Upsilon_{0\alpha} = \frac{\alpha U_{x0}}{\omega_0(k_0)} = \mathfrak{a}\mathfrak{U}_{0\alpha}; \quad \delta_{\alpha 0} = \frac{\mathfrak{a}\mathfrak{U}_{0\alpha}}{\mathfrak{a}+2}. \tag{87}$$

We find from equations (74) and (85) — with (82) and noting that $c(k_0) = \omega_0(k_0)(1-\delta_{\alpha 0})/k_0$ in the Stewart & Joy approximation (23) — that the orbital velocities are approximated by

$$u(x,z,t) \approx \mathrm{Re}\left\{\frac{a\omega_0(k_0)L}{\sqrt{L^2+iB_{0\alpha}t}}\left[1-(1+\mathfrak{a})\delta_{\alpha 0}e^{\alpha z}\right]e^{\Psi_0(x,z,t)}\right\}; \tag{88a}$$

$$v(x,z,t) \approx -\mathrm{Re}\left\{\frac{aU_y'(z)L}{\sqrt{L^2+iB_{0\alpha}t}}e^{\Psi_0(x,z,t)}\right\}; \tag{88b}$$

$$w(x,z,t) \approx \mathrm{Im}\left\{ \frac{a\omega_0(k_0)L}{\sqrt{L^2+iB_{0\alpha}t}}\left[1-\delta_{\alpha 0}e^{\alpha z}\right] e^{\Psi_0(x,z,t)}, \right\} \tag{88c}$$

with the shorthand

$$\Psi_0(x,z,t) = k_0 z + ik_0 x - i\omega(k_0)t - \frac{(x-A_{0\alpha}t)^2}{2(L^2+iB_{0\alpha}t)}, \tag{89}$$

and $\Upsilon_{0\alpha}$ from equation (87). $A_{0\alpha}$ and $B_{0\alpha}$ were given in equation (62). The approximate expression (88a) is compared to the exact analytical expression presented below in section 4.4.2 in figure 13.

The surface amplification is now easily found from equation (88a),

$$\mathrm{amp}_0 = 1 - (1+\mathfrak{a})\,\delta_{\alpha 0}. \tag{90}$$

Equation (88) demonstrates a striking observation mentioned above: when shear is opposing, i.e., $\Upsilon_0 > 0$, the maximum value of u is not necessarily at $z = 0$ but can be positioned below the surface. With the approximate expression (88a), the criterion for the maximum to lie below the surface — that $u'(z) < 0$ at $z = 0$ — is readily found to be

$$(\mathfrak{a}+1)^2\delta_{\alpha 0} > 1 \tag{91}$$

or alternatively

$$\mathfrak{U}_{0\alpha} > \frac{\mathfrak{a}+2}{\mathfrak{a}(\mathfrak{a}+1)^2} \sim \mathfrak{a}^{-2} + ... \tag{92}$$

with the current strength parameter $\mathfrak{U}_{0\alpha}$ from equation (87). The last form is the asymptotic expansion as $\mathfrak{a} \gg 1$, which is good to better than 10% for $\mathfrak{a} \gtrsim 3.5$. A sufficient criterion for (92) to hold valid asymptotically as $\mathfrak{a} \to \infty$ is thus simply that the maximum lies beneath the surface if

$$\mathfrak{a}^2\mathfrak{U}_{0\alpha} > 1. \tag{93}$$

Note that the large-$\mathfrak{a}$ limit is not in contradiction to the weak-shear approximation if $\mathfrak{U}_{0\alpha} \ll 1$ since $\lim_{\mathfrak{a}\to\infty}\delta_{\alpha 0} = \mathfrak{U}_{0\alpha}$.

For $U_{x0} > 0$ the maximum value of u is located where $u'(z) = 0$, provided this occurs at a negative z, otherwise it is at $z = 0$. Differentiating (88a) we find the maximum value at focus to be at level $z_{\max,\alpha}$ and give amplification $\mathrm{amp}_{\max,\alpha}$ as follows,

$$z_{\max,\alpha} = \min\left\{0, -\frac{1}{\alpha}\ln[(\mathfrak{a}+1)^2\delta_{\alpha 0}]\right\}; \tag{94}$$

$$\mathrm{amp}_{\max,\alpha} = \begin{cases} \frac{\mathfrak{a}}{1+\mathfrak{a}}\left[(\mathfrak{a}+1)^2\delta_{\alpha 0}\right]^{-1/\mathfrak{a}}, & \text{if } (\mathfrak{a}+1)^2\delta_{\alpha 0} > 1, \\ 1-(\mathfrak{a}+1)\delta_{\alpha 0}, & \text{otherwise} \end{cases} \tag{95}$$

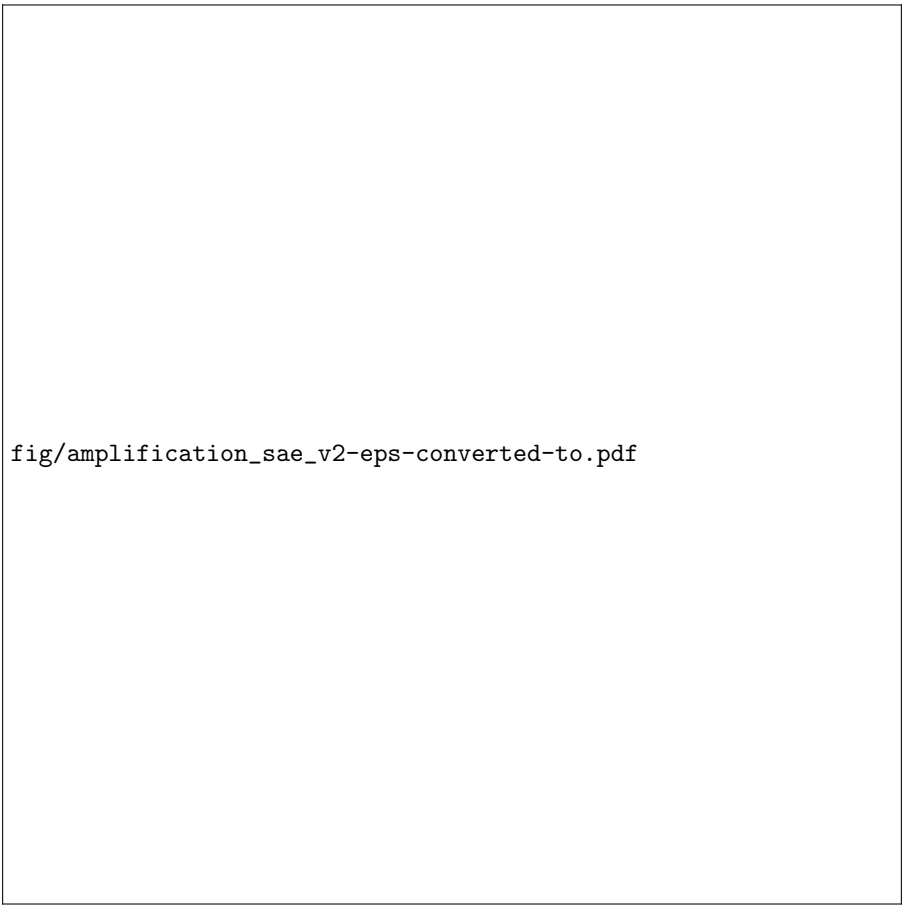

Fig. 11 Velocity amplification for an exponential current. Marker shapes indicate values of $\delta_{\alpha 0}$ as quoted in the legend of panel (a), and graphs and markers are colour coded as the legend in panel (b) shows; both legends are common to all panels; we defined $c_{00} = c_0(k_0)$. The solid lines show the maximum amplification, while the dashed lines of the same colour show the surface amplification (visible only when the two are different). The small black dots show the weak-shear narrowband approximation of equation (95). The insets show the shape of the wave group at focus.

with $\delta_{\alpha 0}$ from equation (87). Asymptotes for $\mathfrak{a} \to \infty$ are

$$\mathrm{amp}_{\max,\alpha} \approx \begin{cases} 1 - \frac{1+\ln(\mathfrak{U}_{0\alpha}\mathfrak{a}^2)}{\mathfrak{a}} + ..., & \mathfrak{U}_{0\alpha} > 0; \\ -\mathfrak{a}\mathfrak{U}_{0\alpha} + 1 + \mathfrak{U}_{0\alpha} + \mathcal{O}(\mathfrak{a}^{-1}) & \mathfrak{U}_{0\alpha} < 0, \end{cases} \tag{96}$$

while

$$\mathrm{amp}_{\max,\alpha} \approx 1 - \tfrac{1}{2}\mathfrak{a}\mathfrak{U}_{0\alpha} + ..., \quad \mathfrak{a} \to 0. \tag{97}$$

Equation (95) is a main result of this paper. Although derived assuming a narrowband wave package, it approximates the velocity amplification to within a few percent already for relatively broadband (short) wave groups, $k_0 L = 2$.

As the inset of figure 11 shows, this Gaussian group is so short as to hardly be referred to as a "group" at all.

The close similarity between the four panels of figure 11 shows with clarity that the amplification factor is essentially determined by two nondimensional groups, the relative current strength $\mathfrak{U}_{0\alpha}$ and the relative shear parameter $\mathfrak{a}$. Moreover, it is striking how closely the simple formulae (95) approximate the numerically calculated amplification for a wide range of parameters of the Gaussian wave group on an exponential profile, even when the underlying assumptions ($k_0 L \gg 1$ and $\delta_{\alpha 0} \ll 1$) are clearly violated.

4.3 Wave kinematics with arbitrary strongly sheared, weakly curved current

When the current $U_{x0}(z)$ is not weakly sheared, i.e., $\delta(\mathbf{k}) \sim \mathcal{O}(1)$, an approximate solution for the vertical velocity is found by applying the method of dominant balance to the Rayleigh equation (65) [20]

$$\tilde{w}(z,t;\ \mathbf{k}) = \tilde{w}_0(0,t;\ \mathbf{k}) \left[e^{kz} - \frac{1}{k} \int_{-\infty}^{z} \mathrm{d}\tilde{z} \frac{U_x''(\tilde{z})}{c(\mathbf{k}) - U_x(\tilde{z})} e^{k\tilde{z}} \sinh k(z-\tilde{z}) \right] \quad (98)$$

with c approximated by equation (24). With (67a) it follows that

$$\tilde{u}(z,t;\ \mathbf{k}) = i\tilde{w}_0(0,t;\ \mathbf{k}) \left[e^{kz} - \frac{1}{k} \int_{-\infty}^{z} \mathrm{d}\tilde{z} \frac{U_x''(\tilde{z})}{c(\mathbf{k}) - U_x(\tilde{z})} e^{k\tilde{z}} \cosh k(z-\tilde{z}) \right]. \quad (99)$$

When $U_x(z)/c \ll 1$ these expressions can be reduced to equations (77) and (81a), respectively, in the latter case noting that $\cosh \xi = -\sinh \xi + 2\exp(\xi)$.

When an exponential current (19) is inserted, the integral can be evaluated in closed form and expressed in terms of a hypergeometric function. However, the resulting expression is no simpler than the exact solution in this case with no restrictions on shear or curvature, presented in 4.4.2. Due to the relative complexity of the analytical expressions we will not pursue the weak-curvature approximation further for the purposes of kinematics.

4.4 Exact linear solutions

Exact solutions to the Rayleigh equation (65) exist for nonzero ω only in special situations [16]. We consider two cases: $\mathbf{U}$ being a linear or exponentially decaying function of z.

4.4.1 Current with linear shear

Consider linear shear, $\mathbf{U}(z) = \{U_x, U_y\} = Sz\{\cos\theta, \sin\theta\}$ and $\omega = \sqrt{\varkappa} - \sigma$, $\varkappa = k + \sigma^2/g$ and $\sigma = \frac{1}{2} S \cos\theta$ as before. The linear-theory orbital velocities for a wave with wave vector $\mathbf{k} = \{k, 0\}$ on such a current are well known. Since $U_x''(z) = 0$, the Rayleigh equation (65) becomes near trivial and following [43]

Fig. 12 Horizontal velocity profiles with linear shear current. The shear profile is expressed as $U_x(z) = 2\sigma z$ with, left to right, $\tilde{\sigma} = \{0.75, 0.5, 0.25, .0.125, 0, -0.125, -0.25, -0.5, -0.75\}$. The wave shape at focus, shown as inset, is $\zeta(x, 0, t)/a = \exp(-\frac{1}{2}x^2/L^2)\cos(k_0 x)$ with $k_0 L = 3$, i.e., a maximum Froude-shear number $|\mathrm{FS}_{\mathrm{lin.}}| = 0.43$ according to equation (18).

(after a rotation of the coordinate system) gives the simple result

$$\tilde{w}(z, t;\ \mathbf{k}) = \tilde{w}(0, t;\ \mathbf{k})e^{kz}; \quad \tilde{u}(z;\ \mathbf{k}) = i\tilde{w}(0, t;\ \mathbf{k})e^{kz}. \tag{100a}$$

This is ostensibly the potential wave solution, which one obtains for a strictly 2-dimensional flow with constant vorticity [43], but note that $\tilde{v}$ is not zero; instead

$$\tilde{v}(z, t;\ \mathbf{k}) = -\frac{iS\sin\theta}{\omega(\mathbf{k}) - kU_x(z)}\tilde{w}(0, t;\ \mathbf{k})e^{kz}. \tag{101}$$

This accords with [43] and describes a shifting and twisting of vortex lines as the plane wave passes. $\tilde{v}$ vanishes when shear is zero or the current is parallel or antiparallel to the wave ($\theta = 0$ or π).

Thus for the focusing wave group one obtains (notice that with our convention, $\mathbf{k} = \{k, 0\}$ with $k > 0$)

$$w(x, z, t) = 2\,\mathrm{Im}\int_0^\infty \frac{\mathrm{d}k}{2\pi}\omega(k)\tilde{\zeta}_0(k)e^{kz}e^{i\psi}; \tag{102a}$$

$$u(x,z,t) = 2\,\mathrm{Re}\int_0^\infty \frac{\mathrm{d}k}{2\pi}\omega(k)\tilde{\zeta}_0(k)e^{kz}e^{i\psi}; \tag{102b}$$

$$v(x,z,t) = -\,2\,\mathrm{Re}\int_0^\infty \frac{\mathrm{d}k}{2\pi}\frac{S\omega(k)\sin\theta}{\omega(k)-kU_x(z)}\tilde{\zeta}_0(k)e^{kz}e^{i\psi}. \tag{102c}$$

At first glance it might seem as if u and w are not much affected by the shear, having as they do the same structure as the expressions sans current. However, the quantitative effect is highly significant, because as previously discussed the frequency ω contained in ψ varies very significantly with the sign of σ when the latter is not very small compared to $\sqrt{gk}$. Thus, being proportional to $\omega(k)$, the orbital velocities u, w can be very significantly greater for $\sigma < 0$ compared to $\sigma > 0$. Secondly an oblique angle between wave and current makes for significant horizontal motion across the wave plane (also true for currents of more general depth profile, provided vertical shear is non-zero, according to equation (67b)).

For the linear profile the velocity is always highest at the surface, hence the velocity amplification is

$$\mathrm{amp}_{\mathrm{lin}} = \frac{\int_0^\infty \mathrm{d}k\,\omega(k)\mathrm{Re}\{\tilde{\zeta}_0(k)\}}{\int_0^\infty \mathrm{d}k\,\omega_0(k)\mathrm{Re}\{\tilde{\zeta}_0(k)\}} \tag{103}$$

with $\omega(k)$ from equation (14). The case of a narrowband wave group is considered in section 4.5, in which case the amplification becomes particularly simple.

The qualitative difference in behaviour during focusing and defocusing was illustrated in figures 2 and 3. Figure 12 shows the horizontal velocity profiles beneath the focus point, $u(0,z,0)$ for linear shear currents of different strengths, for a Gaussian wave group with $k_0L = 3$. The qualitative shape of u remains the same, except amplified. The surface amplification varies between approximately 0.65 and 1.52 for the strongest opposing and following shear, respectively.

4.4.2 Current with exponential shear

In the case of an exponential current (19), Hughes & Reid [44] showed that the Rayleigh equation (65) permits the exact solution (see also [45] and Appendix B of [46])

$$\tilde{w}(z,t;\ k) = \tilde{W}(t;\ k)\,{}_2F_1(\mathcal{A}_-,\mathcal{A}_+;\ \mathcal{R};\ \mathcal{W}(z))e^{kz} \tag{104}$$

with ${}_2F_1$ being the hypergeometric function, $\tilde{W}(t,k)$ follows from free-surface boundary conditions, and

$$\mathcal{A}_\pm = (k \pm \sqrt{\alpha^2+k^2})/\alpha; \quad \mathcal{R} = 1 + 2k/\alpha; \quad \mathcal{W}(z) = \frac{kU_{x0}e^{\alpha z}}{\omega + kU_{x0}}. \tag{105}$$

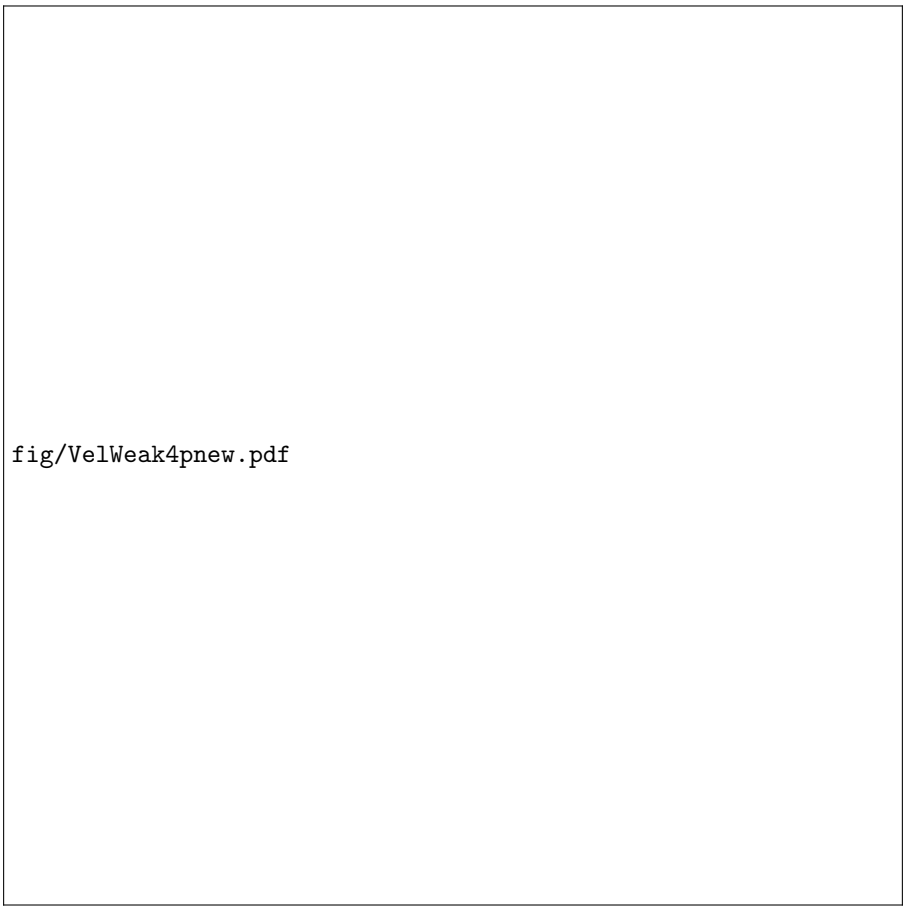

Fig. 13 Horizontal orbital velocity profiles at focus, $u(0,z,0)$, normalised by the surface value without shear, for a medium-bandwidth focusing wave, $k_0L = 3$ (a) and $k_0L = 5$ (b) on an exponential current, equation (19). Insets show the wave group shape at focus. Here $U_{x0} = 0.2\,U_{\rm ref}$ (solid lines) and $-0.2\,U_{\rm ref}$ (dashed lines). Comparison of exact solution [equations (67a) and (106)] (black lines) and the weak-shear narrowband approximation (red lines), equation (88). The values on the top of each curve refer to α/k_0.

The horizontal velocity $\tilde{u}(z,t;\ k)$ is found from equations (67), $u = i\tilde{w}'/k$, giving

$$\tilde{w}'(z) = k\tilde{w}(z) - \frac{\alpha k U_{x0}\tilde{W}(t;\ k)}{(\omega + kU_{x0})\mathcal{R}}\, e^{(k+\alpha)z}\, {}_2F_1(\mathcal{A}_- + 1, \mathcal{A}_+ + 1;\ \mathcal{R}+1, \mathcal{W}(z)) \quad (106)$$

The dispersion relation to find $\omega(k)$ is implicit, given by the combined free-surface boundary condition (see [26])

$$\omega^2\tilde{w}'(0) - k(gk - \omega\alpha U_{x0})\tilde{w}(0) = 0. \quad (107)$$

whose solution $\omega(k)$ is readily found numerically. Alternatively we may apply the Direct Integration Method [26] directly.

The solutions (104) and (106) are exact for linear waves regardless of how strongly sheared the current is. The comparison of the exact solution using the theory in this section and the approximate solution in section 4.2.1 is shown in figure 13. The results demonstrate that the approximate expression gives fairly accurate solution given a relatively weak shear current. Although the exact solution (106) can be used without difficulty, the computation of the hypergeometric function can be time consuming. Therefore, one may consider the approximate expression instead.

4.5 Surface velocity amplification for long, Gaussian groups

Consider the case of a long, or narrowbanded, Gaussian group with carrier wavenumber k_0, as considered in section 3.4, i.e., $\tilde{\zeta}_0(k)/a = \sqrt{\pi/2}L\exp[\frac{1}{2}(k - k_0)^2L^2]$, where $k_0 \gg 1$ (as we have seen, $k_0L \sim 5$ is sufficiently large). At $x = z = t = 0$ the integrals in equation (72) now particularly simple in the Laplace approximation, and we obtain

$$\mathrm{amp}_0 \approx \frac{c(k_0)}{c_0(k_0)}\left[1 + \frac{1}{k_0}f'(0;\ k_0)\right]. \tag{108}$$

In other words a typical value of the amplification is, to leading order, the ratio of phase velocities at the carrier frequency with and without shear, which as discussed in section 3.1 can vary greatly for realistic shear currents, with a currection term playing a role if the profile $U_x(z)$ has significant curvature.

In particular, for linear shear $U_x(z) = Sz$, we have $f'(z) = 0$ (e.g. [17]) and with (14),

$$\mathrm{amp}_{\mathrm{lin.shear}} \approx \sqrt{1 + \frac{\sigma^2}{\omega_0^2}} - \frac{\sigma}{\omega_0} = \sqrt{1 + \mathrm{FS}_{\mathrm{lin.}}^2\cos^2\theta} - \mathrm{FS}_{\mathrm{lin.}}\cos\theta \tag{109}$$

where the shear-Froude number was defined in (18), taken here at $k = k_0$. This accords with equation (26) which was based on the difference in phase velocity only.

4.5.1 Velocity and amplification in real conditions: the Columbia River Estuary

We consider now the current and wave climate measured in the estuary of the Columbia River, as detailed in section 3.4.4. To make the study as realistic as possible, we devise a focusing wave based on the wave spectrum reported in reference [38] and generate a wave field from this. The power spectrum we use is shown in figure 14 (a).

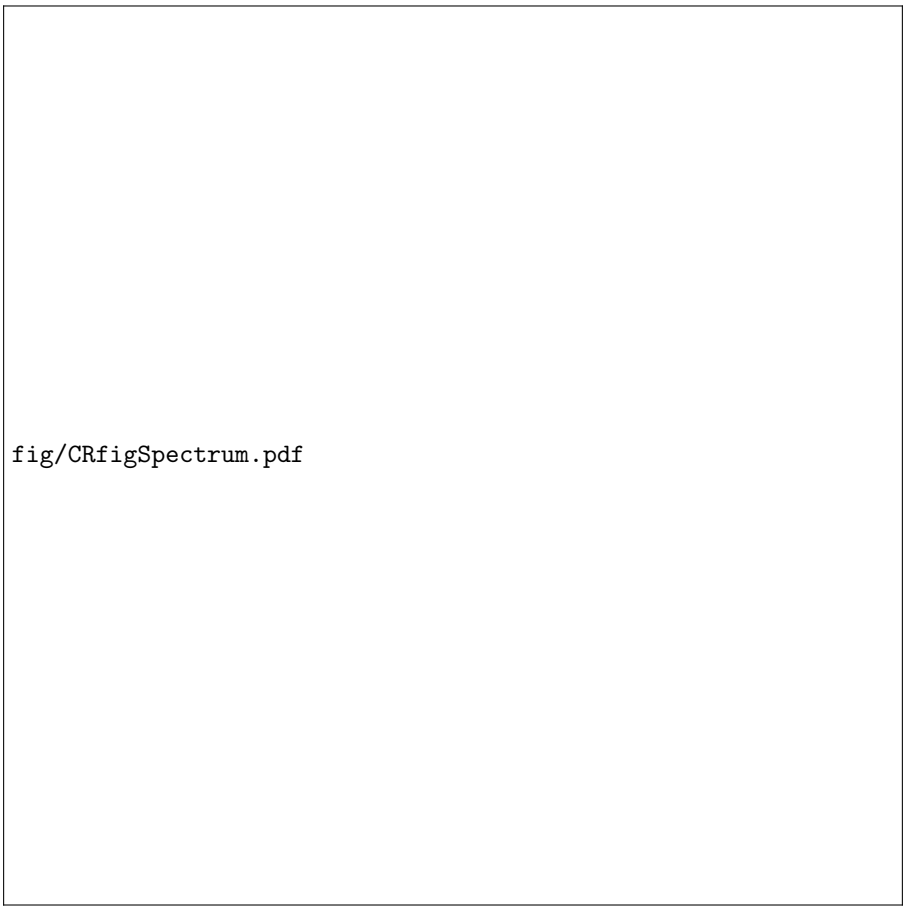

Fig. 14 (a) Power energy spectrum measured in the Columbia River delta [38], (b) intial-value spectrum $\tilde{\zeta}_0(k)$ based on $S(f)$. Circular markers: measured data. Solid line: fitted function.

We devise a smooth initial-value spectrum $\tilde{\zeta}_0(k)$ based on the measured wave spectrum $S(f)$ with $f = \omega/2\pi$ is the wave frequency in cycles per second. In this paragraph only, we use dimensional units without an asterisk. Unlike for generating a random sea state [47], for a focusing wave group we can obtain an initial wave elevation spectrum $\tilde{\zeta}_0(k)$ which resembles that which is measured, as follows. The discrete measured values $\{f_i, S_i\}$ are transformed to a set of discrete value pairs $\{k_i, \tilde{\zeta}_i\}$,

$$\sqrt{2S_i\Delta f} = \tilde{\zeta}_i \Delta k \tag{110a}$$

$$\tilde{\zeta}_i = \frac{\sqrt{2S_i\Delta f}}{\Delta\omega}\left(\frac{\mathrm{d}\omega}{\Delta k}\right)_i = \frac{\sqrt{2S_i\Delta f}}{4\pi^2\,\Delta f}\frac{g}{2f_i} \tag{110b}$$

where we used $\Delta\omega/\Delta k \approx \mathrm{d}\omega/\mathrm{d}k$, Δf is the distance between frequency values f_i, and we used $\omega = \sqrt{gk}$. We finally fit the set of points $\{k_i, \tilde{\zeta}_i\}$ to the spectrum of a broadband Gaussian group, (51), $\tilde{\zeta}_0(k) = \sum_{\pm} a \exp[-L^2(k \pm k_0)^2/2]$, which gives $k_0 = 0.13\,\mathrm{rad/m}$ and $1/L = 0.087/\mathrm{m}$The measured spectrum $S(\omega)$ is shown in panel (a) of figure 14, and the smooth $\tilde{\zeta}_0(k)$ is plotted along with the measurements, transformed with equation (110b) in figure 14(b).

The governing nondimensional parameters are thus $\mathfrak{U}_{0\alpha} = 0.18$, $\mathfrak{a} = 2.03$ (ZT) and $\mathfrak{U}_{0\alpha} = 0.16$, $\mathfrak{a} = 3.05$ (KN). The shear-Froude number for current ZT and KN are $\delta_{\alpha 0} = 0.092$ and 0.095, respectively, so although these currents are frequently referred to as very strongly sheared in the context of natural flows [31, 34, 35], the conditions lie safely in the weak-shear regime where Stewart & Joy's approximation (sections 2.4.1 and 4.2) can be used. Moreover, although the wave shape at focus is so broadband as to hardly be called a group (resembling the shape in the inset of figure 11a), the narrow-band approximation (88a) is an excellent approximation to the velocity profiles at focus.

The resulting horizontal orbital velocity profile $u(z, 0, 0)$ at focus is shown in figure 15(a) for the wave group propagating downstream, across and upstream on the Columbia River current as seen by an earth-fixed observer, corresponding to, respectively, maximally opposing, zero and maximally following shear, i.e., $\theta = 0$, $\theta = \pi/2$ and $\theta = \pi$. (Bear in mind that velocities in our formalism are measured in the system following the mean surface velocity; see figure 9).

The surface shape at focus is identical by construction, and the envelope of the focusing and defocusing groups are virtually indistinguishable, yet the difference in maximum orbital velocity is dramatic. The wave-induced orbital velocity beneath the focus point, $u(0, 0, 0)$, is increased and reduced by factors of approximately 1.4 and 0.7 compared to the no-shear case for groups propagating upstream and downstream on the river, respectively. This corresponds to the wave-induced dynamic pressure, at $x = t = 0$, $p_{\mathrm{dyn}} = \frac{1}{2}\rho u^2$, being approximately doubled and halved, respectively, very significantly affecting the force exerted on vessels and constructions. (For balance is worth bearing in mind that waves propagating against the current are typically higher than those propagating downstream in this location [38]).

5 Conclusions

We have considered the linearised theory of focusing long-crested wave groups on shear currents of arbitrary vertical depth dependence, allowing an arbitrary angle between the current and wave propagation. Although limited in steepness, a number of insights into the way groups of waves focus and defocus can be gained. We derive a large number of approximate relations which can explicitly reveal the underlying physics, while at the same time being useful tools in their own right, for instance for the generation of focusing wave groups in a wave tank along the lines of [15].

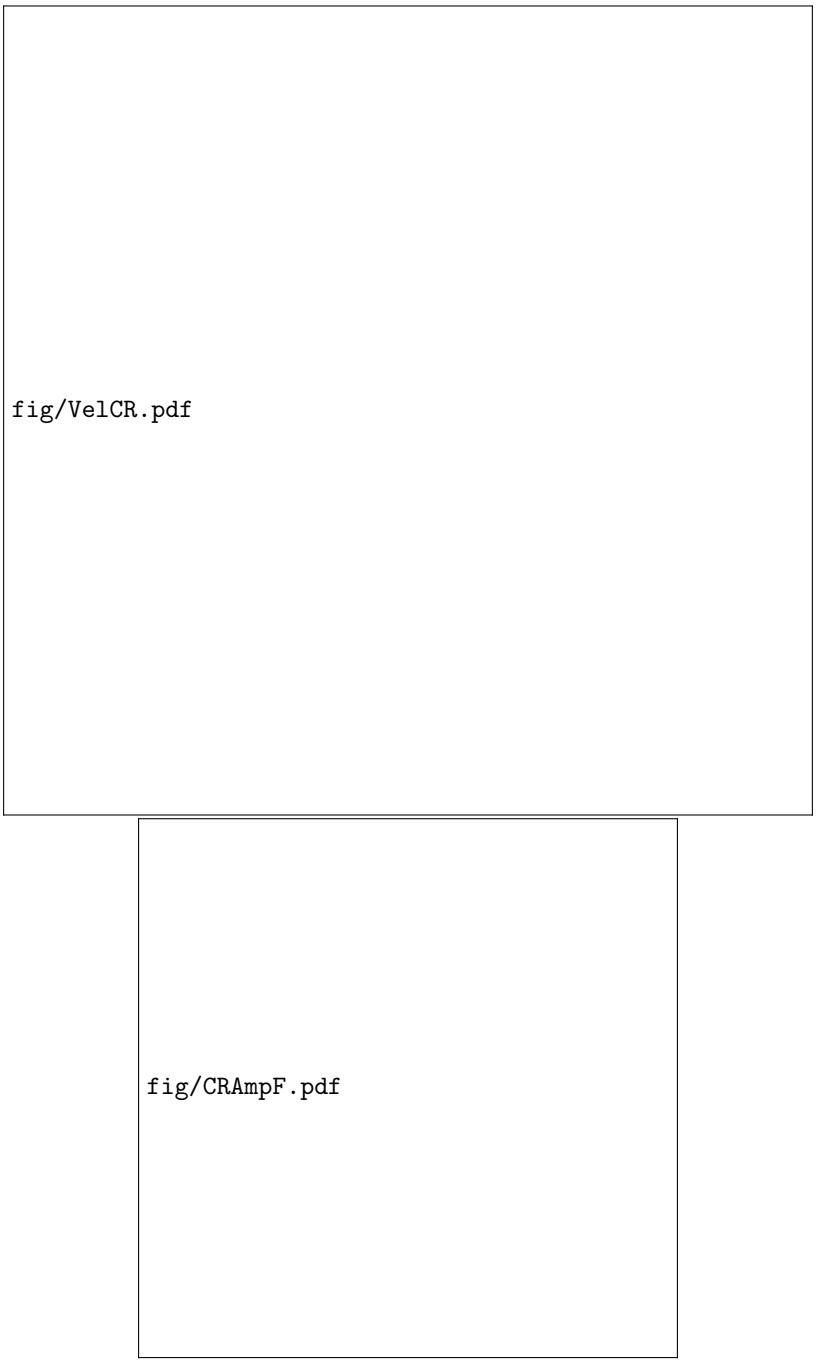

Fig. 15 Top: Horizontal orbital velocity $u(0, z, 0)$ beneath the focus of a medium-bandwidth Gaussian group ($k_0 L = 1.48$) in the presence of measured currents in the Columbia River Estuary, as measured by Zippel & Thomson (ZT, [38]) and Kilcher & Nash (KN, [39]), shifted so that $U(0) = 0$ and approximated by exponentials $U(z) = U_0[\exp(\alpha z) - 1]$. Values for $|U_{x0}|, \alpha, \mathfrak{a}$ and $\delta_{\alpha 0}$ for ZT and KN are found in the main text. Black lines show 'exact' numerical solutions, red lines are the weak-shear-narrowband approximation, equation (88a). Solid, thick, and dashed lines refer to $\cos\theta = 0, \pi/2$ and π, respectively. Bottom: velocity amplification as a function of the angle θ between wave propagation direction and current for the same two velocity profiles.

Particular attention is paid to two groups of currents: the current varying linearly with depth, and currents of arbitrary depth dependence whose effect on waves may be approximated using the theory by Stewart & Joy's [14] and others, the criterion for which is that the depth-averaged shear is, in the appropriate sense, sufficiently weak. For the linear current, exact and readily tractable solutions exist, allowing several classical results without shear to be generalised. The "weak-shear" assumption behind the latter class of currents is not a significant limitation in practice, since the vast majority of oceanographic currents and wave spectra satisfy the appropropriate criterion of validity. For instance in the Columbia River delta which we consider as an example, the shear is frequently described as being very strongly sheared [31, 34, 35], yet remains safely within the weak-shear assumption's range of validity. The assumption is already in widespread use in ocean modelling (e.g. [35]).

For the much used model of a current profile varying exponentially with depth — modelled as $U(z) = U_0[e^{\alpha z} - 1]$ with $\alpha > 0$ — the weak-shear approximation yields a number of broadly applicable, simple and closed-form approximate relations for the surface elevation of a progressing wave group, and its concomitant orbital velocity field.

Particular attention is paid to Gaussian wave groups which at focus takes the shape of a carrier wave (wavenumber k_0) with a Gaussian envelope of width L: $\zeta_0(x) \propto \exp(-\frac{1}{2}x^2/L^2)\cos k_0 x$. Assuming a long group — i.e., narrowband in Fourier space — we may derive a wealth of relations which can describe a wide range of realistic situations. Strikingly, the group does not need to be particularly long (or narrowband): the narrowband results are excellent for most practical purposes already $k_0 L = 3$, a group which at the point of focus mainly consists of a single tall crest with deep troughs either side.

A key observation from studying the developing wave group is that while the shear current has modest effect on the evolution of the group envelope, the behaviour inside the group is far more affected. In opposing shear individual crests rise slowly and take longer to traverse the length of the group, while following shear causes the wave behaviour inside the group to appear more volatile, with individual crests and troughs rising and falling more rapidly.

Regarding the orbital wave motion beneath the surface, this difference in behaviour depending on the direction of sub-surface shear becomes even more important. For following shear, horizontal orbital velocities are significantly amplified compared to the case sans shear, and reduced in opposing shear. The amplification can significantly alter the wave forces acting on a body encountering the focusing group.

We derive a simple approximate relation for the velocity amplification beneath the focus point of a Gaussian wave group atop an exponential velocity profile, as a function of two nondimensional groups of parameters: the relative current strength $U_0\sqrt{k_0/g}$, and the vertical vs horizontal rate of variation, α/k_0.

For illustration of these observed phenomena in a practical setting we have considered waves in the mouth of the Columbia River, where depth-resolved current measurements as well as measured wave spectra are available [38, 39]. For a focusing wave with the same spectrum as that measured, i.e., having the same surface elevation $\zeta(x,0)$ at the point of focus, the horizontal orbital velocity beneath the crest is increased by approximately 40% for following shear (i.e., propagating upstream in an earth-fixed frame) compared to a depth-uniform current, whereas for opposing shear (downstream propagation) the amplitude is reduced by about a factor 0.72. This corresponds to the wave-induced dynamic pressure being approximately doubled and halved, respectively, greatly affecting the forces such a focused group will exert on vessels and structures.

A Linear focusing theory in shallow water

A.1 Linear shear

The dispersion relation with finite depth h is now (e.g. [43]),

$$\omega(k) = \sqrt{gk\tanh kh + \left(\sigma\tanh kh\right)^2} - \sigma\tanh kh. \tag{111}$$

Following Refs. [25, 28], the surface elevation integral (11) can be solved approximately in shallow water by expanding $\omega(k)$ in powers of h and k

$$\begin{aligned}\omega(k) =& kc_h - k\sigma h + \tfrac{1}{2}k\sigma^2 g^{-\frac{1}{2}}h^{\frac{3}{2}} - g^{-\frac{3}{2}}(\tfrac{1}{6}g^2k^3 + \tfrac{1}{8}k\sigma^4)h^{\frac{5}{2}} \\ &+ \tfrac{1}{3}k^3\sigma h^3 - g^{-\frac{3}{2}}\sigma^2(\tfrac{1}{4}g^2k^2 - \tfrac{1}{16}\sigma^4)h^{\frac{7}{2}} + \mathcal{O}(h^{\frac{9}{2}}) \qquad (112a)\\ \equiv& w_1 k - \tfrac{1}{3}w_3k^3 + ... \qquad (112b)\end{aligned}$$

with

$$\begin{aligned}w_1 =& c_h - h\sigma + \tfrac{1}{2}\sigma^2 g^{-\frac{1}{2}}h^{\frac{3}{2}} - \tfrac{1}{8}g^{-\frac{3}{2}}k\sigma^4 h^{\frac{5}{2}} + \mathcal{O}(h^3); \qquad (113a)\\ w_3 =& \tfrac{1}{2}c_h h^2 - \sigma h^3 + \mathcal{O}(h^{\frac{7}{2}}), \qquad (113b)\end{aligned}$$

where $c_h = \sqrt{gh}$ is the phase (and group) velocity in the shallow-water limit in absence of a shear current.

A.2 δ-function singularity in shallow water with linear current profile

Consider the case of a group focusing to the delta function singularity, equation (47), where the expansion (111) is inserted. We shall need the linear and cubic in k.

Evaluating the integral (47), the surface shape at any time t is then, approximately,

$$\zeta(x,t) = \frac{aL}{(w_3 t)^{1/3}} \mathrm{Ai}\left[\frac{x - w_1 t}{(w_3 t)^{1/3}}\right]. \tag{114}$$

This is a direct generalisation of the result of refs. [25, 28] including a constant shear.

A.3 Gaussian wave group, arbitrary depth

For linear shear S and general depth h, the expressions for $A_0 = \omega'(k_0)$ and $B_0 = \omega''(k_0)$ which may be inserted into (56) are

$$A_0 = -\frac{h\sigma}{\mathcal{C}_0^2} + \frac{\mathcal{C}_0\mathcal{S}_0 + (2\varkappa - k_0)h}{2\mathcal{C}_0^2\sqrt{\mathcal{T}_0}}\sqrt{\frac{g}{\varkappa}}; \tag{115a}$$

$$B_0 = \frac{2h^2\sigma\mathcal{T}_0}{\mathcal{C}_0^2} - \sqrt{g\varkappa\mathcal{T}_0}\left[\frac{1}{4\varkappa^2}\left(\frac{hk_0}{\mathcal{C}_0\mathcal{S}_0} - 1\right)^2 + \frac{h^2}{\mathcal{C}_0^2}\left(2 - \frac{k_0}{\varkappa}\right)\right], \tag{115b}$$

with shorthand

$$\mathcal{C}_0 \equiv \cosh k_0 h, \quad \mathcal{S}_0 \equiv \sinh k_0 h, \quad \mathcal{T}_0 \equiv \tanh k_0 h = \mathcal{S}_0/\mathcal{C}_0, \tag{116}$$

and shear-modified wave number

$$\varkappa = k_0 + \sigma^2\mathcal{T}_0/g \longrightarrow \begin{cases} k_0 + \sigma^2/g & k_0 h \to \infty \\ k_0(1 + \sigma^2 h/g) & k_0 h \to 0 \end{cases}. \tag{117}$$

(Note $\omega(k_0) = \sqrt{g\varkappa\mathcal{T}_0} - \sigma\mathcal{T}_0$ in this formalism).

In the shallow water regime, $k_0 h \equiv \xi_0 \ll 1$ we obtain

$$A_0 = \sqrt{gh} - v_\sigma\xi_0 + \tfrac{1}{2}(v_\sigma^2/c_{00})\xi_0^{\frac{3}{2}} - \tfrac{1}{2}c_{00}(1 + \tfrac{1}{4}v_\sigma^4/c_{00}^4)\xi_0^{\frac{5}{2}} + v_\sigma\xi_0^3 + \ldots \tag{118a}$$

$$k_0 B_0 = -c_{00}\xi_0^{\frac{5}{2}} + 2v_\sigma\xi_0^3 + \ldots \tag{118b}$$

with $c_{00} = c_0(k_0) = \sqrt{g/k_0}$ and $v_\sigma = \sigma/k_0$. For example, from equation (56) one sees that for a Gaussian package the time it takes for the group to change significantly is $t \sim L^2/B_0 \approx (k_0 L^2/c_{00})\xi_0^{-\frac{5}{2}}$, by which time the group has traveled of order $A_0 t/\lambda_0 \sim (k_0^2 L^2/2\pi)\xi_0^{-2}$ wavelengths of the carrier wave. However, notice that the leading-order correction to the phase and group velocities are order $\mathrm{FS}_{\mathrm{lin.}}\xi_0^{\frac{1}{2}}$ and can be significantly affected by the shear even when ξ_0 is not extremely small. This is illustrated in Figure 16 in moderately shallow water, $\xi_0 = 0.2$: The group at focus (red graph) does not change shape perceptibly, but the phase velocity is clearly increased for $\sigma < 0$ and decreased for $\sigma > 0$.

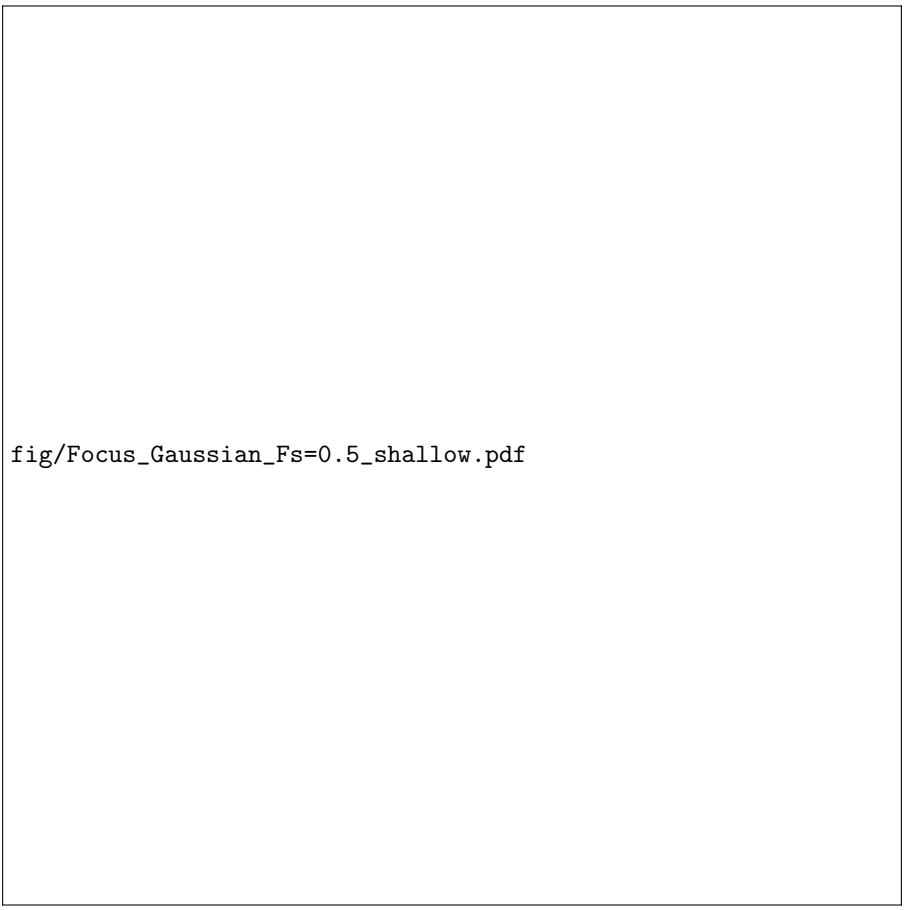

Fig. 16 Waves focusing into a group with a Gaussian envelope in moderately shallow water, $k_0h = 0.2$. The solid graphs show $\eta(x,t)/a$ for $\sqrt{gk_0}t$ from -45 to 45 in steps of 0.5 with the shape at $t = 0$ shown in red. Here $S = \sqrt{gk_0}$, $k_0L = 3$, and $\theta = 0$ (top), $\pi/2$ (centre) and π (bottom).

Conflict of interest. corresponding author avers that there is no conflict of interest.

Data availability. No new data was generated in the research reported, and all equations necessary to reproduce the results are included.

Acknowledgments. SÅE was supported in part by the European Union (ERC, WaTurSheD, project 101045299) and the Research Council of Norway (project 325114). ZZ acknowledges the support from China Scholarship Council through project 201906060137. YL acknowledges the financial support from the Research Council of Norway through a FRIPRO mobility grant (project no. 287398) and a POS-ERC grant (project no. 342480). Views and opinions expressed are those of the authors only and do not necessarily reflect those of

the European Union or the European Research Council. Neither the European Union nor the granting authority can be held responsible for them.

References

[1] Kharif, C., Pelinovsky, E.: Physical mechanisms of the rogue wave phenomenon. European Journal of Mechanics-B/Fluids **22**(6), 603–634 (2003)

[2] Dysthe, K., Krogstad, H.E., Müller, P.: Oceanic rogue waves. Annu. Rev. Fluid Mech. **40**, 287–310 (2008)

[3] Onorato, M., Residori, S., Bortolozzo, U., Montina, A., Arecchi, F.: Rogue waves and their generating mechanisms in different physical contexts. Physics Reports **528**(2), 47–89 (2013)

[4] Johannessen, T.B., Swan, C.: A laboratory study of the focusing of transient and directionally spread surface water waves. Proceedings of the Royal Society A: Mathematical, Physical and Engineering Sciences **457**(2008), 971–1006 (2001)

[5] Brown, M.G., Jensen, A.: Experiments on focusing unidirectional water waves. Journal of Geophysical Research: Oceans **106**(C8), 16917–16928 (2001)

[6] Grue, J., Clamond, D., Huseby, M., Jensen, A.: Kinematics of extreme waves in deep water. Applied Ocean Research **25**(6), 355–366 (2003)

[7] Vyzikas, T., Stagonas, D., Buldakov, E., Greaves, D.: The evolution of free and bound waves during dispersive focusing in a numerical and physical flume. Coastal Engineering **132**, 95–109 (2018)

[8] Adcock, T.A.A., Taylor, P.H.: Focusing of unidirectional wave groups on deep water: an approximate nonlinear schrödinger equation-based model. Proceedings of the Royal Society A: Mathematical, Physical and Engineering Sciences **465**(2110), 3083–3102 (2009)

[9] Kharif, C., Pelinovsky, E., Talipova, T., Slunyaev, A.: Focusing of nonlinear wave groups in deep water. JETP Letters **73**, 170–175 (2001)

[10] Kharif, C., Abid, M., Touboul, J.: Rogue waves in shallow water in the presence of a vertically sheared current. Journal of Ocean Engineering and Marine Energy **3**(4), 301–308 (2017)

[11] Xin, Z., Li, X., Li, Y.: Coupled effects of wave and depth-dependent current interaction on loads on a bottom-fixed vertical slender cylinder. Coastal Engineering, 104304 (2023)

[12] Zheng, Z., Li, Y., Ellingsen, S.Å.: Dispersive wave focussing on a shear current. Part 2: Weakly nonlinear theory. Submitted manuscript (2023)

[13] Touboul, J., Kharif, C.: Effect of vorticity on the generation of rogue waves due to dispersive focusing. Natural Hazards **84**(2), 585–598 (2016)

[14] Stewart, R.H., Joy, J.W.: HF radio measurements of surface currents. Deep Sea Research and Oceanographic Abstracts **21**(12), 1039–1049 (1974). Elsevier

[15] Clauss, G.F., Bergmann, J.: Gaussian wave packets: a new approach to seakeeping tests of ocean structures. Applied Ocean Research **8**(4), 190–206 (1986)

[16] Peregrine, D.H.: Interaction of water waves and currents. Advances in Applied Mechanics **16**, 9–117 (1976)

[17] Ellingsen, S.Å.: Initial surface disturbance on a shear current: The Cauchy-Poisson problem with a twist. Physics of Fluids **26**(8), 082104 (2014)

[18] Akselsen, A.H., Ellingsen, S.: Weakly nonlinear transient waves on a shear current: Ring waves and skewed Langmuir rolls. Journal of Fluid Mechanics **863**, 114–149 (2019)

[19] Abdullah, A.J.: Wave motion at the surface of a current which has an exponential distribution of vorticity. Annals of the New York Academy of Sciences **51**(3), 425–441 (1949)

[20] Ellingsen, S.A., Li, Y.: Approximate dispersion relations for waves on arbitrary shear flows. Journal of Geophysical Research: Oceans **122**(12), 9889–9905 (2017)

[21] Skop, R.A.: Approximate dispersion relation for wave-current interactions. Journal of Waterway, Port, Coastal, and Ocean Engineering **113**(2), 187–195 (1987)

[22] Kirby, J.T., Chen, T.-M.: Surface waves on vertically sheared flows: approximate dispersion relations. Journal of Geophysical Research: Oceans **94**(C1), 1013–1027 (1989)

[23] Bender, C.M., Orszag, S., Orszag, S.A.: Advanced Mathematical Methods for Scientists and Engineers I: Asymptotic Methods and Perturbation Theory vol. 1. Springer, New York (1999)

[24] Banihashemi, S., Kirby, J.T., Dong, Z.: Approximation of wave action flux velocity in strongly sheared mean flows. Ocean Modelling (2017)

[25] Pelinovsky, E., Talipova, T., Kurkin, A., Kharif, C.: Nonlinear mechanism of tsunami wave generation by atmospheric disturbances. Natural Hazards and Earth System Sciences **1**(4), 243–250 (2001)

[26] Li, Y., Ellingsen, S.Å.: A framework for modelling linear surface waves on shear currents in slowly varying waters. Journal of Geophysical Research: Oceans **124**, 2527–2545 (2019)

[27] Morse, P.M., Feshbach, H.: Methods of Theoretical Physics, Pt 1. McGraw-Hill, New York (1953)

[28] Pelinovsky, E., Talipova, T., Kharif, C.: Nonlinear-dispersive mechanism of the freak wave formation in shallow water. Physica D: Nonlinear Phenomena **147**(1-2), 83–94 (2000)

[29] Neumann, G., Pierson, W.J.J.: Principles of Physical Oceanography. Prentice Hall, Englewood Cliffs, N.J. (1966)

[30] Magnusson, A.K., Donelan, M.A., Drennan, W.M.: On estimating extremes in an evolving wave field. Coastal Engineering **36**(2), 147–163 (1999)

[31] Dong, Z., Kirby, J.T.: Theoretical and numerical study of wave-current interaction in strongly-sheared flows. Coast. Engn. Proc. **1**, 2 (2012)

[32] Gonzalez, F.I., Rosenfeld, C.: Slar and in situ observations of ocean swell modification by currents and bathymetry at the Columbia River entrance. IEEE Transactions on Geoscience and Remote Sensing (6), 598–602 (1984)

[33] Moritz, H.R., Gelfenbaum, G.R., Kaminsky, G.M., Ruggiero, P., Oltman-Shay, J., Mckillip, D.J.: Implementing regional sediment management to sustain navigation at an energetic tidal inlet. In: Kraus, N.C., Rosati, J.D. (eds.) Sixth International Symposium on Coastal Engineering and Science of Coastal Sediment Process, pp. 1768–1786. American Society of Civil Engineers, Reston, VA (2007). https://doi.org/10.1061/9780784409268

[34] Kassem, S., Özkan-Haller, H.T.: Forecasting the wave-current interactions at the mouth of the Columbia River, OR, USA. Coastal Engineering Proceedings **1**(33), 53 (2012). https://doi.org/10.9753/icce.v33.waves.53

[35] Elias, E.P., Gelfenbaum, G., Van der Westhuysen, A.J.: Validation of a coupled wave-flow model in a high-energy setting: The mouth of the Columbia River. Journal of Geophysical Research: Oceans **117**(C9) (2012)

[36] Campana, J., Terrill, E.J., de Paolo, T.: The development of an inversion

technique to extract vertical current profiles from X-band radar observations. Journal of Atmospheric and Oceanic Technology **33**(9), 2015–2028 (2016)

[37] Akan, Çiğdem, Moghimi, S., Özkan-Haller, H.T., Osborne, J., Kurapov, A.: On the dynamics of the Mouth of the Columbia River: Results from a three-dimensional fully coupled wave-current interaction model. Journal of Geophysical Research: Oceans **122**(7), 5218–5236 (2017)

[38] Zippel, S., Thomson, J.: Surface wave breaking over sheared currents: Observations from the mouth of the Columbia River. Journal of Geophysical Research: Oceans **122** (2017)

[39] Kilcher, L.F., Nash, J.D.: Structure and dynamics of the Columbia River tidal plume front. J. Geophys. Res.: Oceans **115**(C5) (2010)

[40] Shrira, V.I.: Surface waves on shear currents: solution of the boundary-value problem. Journal of Fluid Mechanics **252**, 565–584 (1993)

[41] Morland, L.C., Saffman, P.G., Yuen, H.C.: Waves generated by shear layer instabilities. Proceedings of the Royal Society of London. Series A **433**(1888), 441–450 (1991)

[42] Zakharov, V.E., Shrira, V.I.: Formation of the angular spectrum of wind waves. Soviet physics, JETP **71**, 1091–1100 (1990)

[43] Ellingsen, S.Å.: Oblique waves on a vertically sheared current are rotational. European Journal of Mechanics-B/Fluids **56**, 156–160 (2016)

[44] Hughes, T.H., Reid, W.H.: On the stability of the asymptotic suction boundary-layer profile. Journal of Fluid Mechanics **23**(4), 715–735 (1965)

[45] Abid, M., Kharif, C.: Free surface water-waves generated by instability of an exponential shear flow. Submitted manuscript, in review. https://arxiv.org/abs/2305.11983 (2023)

[46] Morland, L., Saffman, P.: Effect of wind profile on the instability of wind blowing over water. Journal of Fluid Mechanics **252**, 383–398 (1993)

[47] Tucker, M., Challenor, P.G., Carter, D.: Numerical simulation of a random sea: a common error and its effect upon wave group statistics. Applied ocean research **6**(2), 118–122 (1984)